HYDRAULIC EFFICIENCY OF A HYDROSTATIC TRANSMISSION WITH A VARIABLE DISPLACEMENT PUMP AND MOTOR

A Thesis presented to the Faculty

of the Graduate School at the

University of Missouri-Columbia

In Partial Fulfillment

of the Requirements for the Degree

Master of Science

---

by

DANIEL COOMBS

Dr. Roger Fales, Thesis Supervisor

DECEMBER 2012

The undersigned, appointed by the Dean of the Graduate School, have examined the thesis entitled

HYDRAULIC EFFICIENCY OF A HYDROSTATIC TRANSMISSION

WITH A VARIABLE DISPLACEMENT PUMP AND MOTOR

Presented by Daniel Coombs

A candidate for the degree of Master of Science

And hereby certify that, in their opinion, it is worthy of acceptance.

Dr. Roger Fales

Dr. Noah Manring

Dr. Stephen Montgomery-Smith

… to my wife, Jill, for all her love and support.

ACKNOWLEDGEMENTS

I would like to thank Dr. Roger Fales for his assistance and contribution to my research. Dr. Fales introduced me to both hydraulics and control systems as an undergraduate at MU. The completion of my Master's degree would not have been possible without his guidance and participation. I would also like to thank Dr. Noah Manring and Dr. Stephen Montgomery-Smith for taking the time to serve on my thesis committee. I would like to thank Richard Carpenter, Tim Keim, Joe Kennedy, Bradley Krone, and Erik Pierce for all of their help and suggestions throughout my research. I am grateful for the high level of mutual respect that exists between us and allows our group to function so well together. I would like to thank the faculty of the Mechanical and Aerospace department at MU for helping me to excel in my field of interest.

TABLES OF CONTENTS

LIST OF FIGURES

LIST OF TABLES

LIST OF SYMBOLS

α	swash plate angle
α_{max}	maximum swash plate angle
A	low frequency error
β	effective fluid bulk modulus
β_a	bulk modulus of air
β_c	bulk modulus of the container
β_l	bulk modulus of liquid
b_{eq}	equivalent viscous drag coefficient
C_c	Coulomb friction torque losses
C_h	hydrodynamic torque losses
C_l	fluid compressibility effects and low-Reynolds-number leakage
C_s	starting torque losses
C_t	high-Reynolds-number leakage
D_m	motor volumetric displacement
D_p	pump volumetric displacement
η	overall efficiency
η_t	torque efficiency
η_v	volumetric efficiency
E	energy
E_{in}	energy input to the system

E_{out}	energy output by the system
J_{eq}	equivalent moment of inertia of the rotating mass
K	leakage coefficient
K_{Hinf}	H_∞ controller
K_o	secant bulk modulus of the liquid
K_{PID}	PID controller
μ	fluid viscosity
M	high frequency error
m	slope of increase
ω	angular velocity
$\dot{\omega}$	angular acceleration
ω_B	bandwidth frequency
P	pressure
P	generalized plant model P
P	power
P_h	hose pressure
$\dot{P}_h$	hose pressure-rise rate
P_{in}	power input to the system
P_{out}	power output by the system
Q	volumetric flow rate
Q_{leak}	leakage volumetric flow rate
Q_m	motor volumetric flow rate

Q_p pump volumetric flow rate

r speed ratio between pump and motor

T input torque

T_{load} load torque

T_m torque produced by motor

T_{out} output torque

V_d volumetric displacement of pump or motor per revolution

w_A additive uncertainty transfer function

w_I multiplicative uncertainty transfer function

w_P performance weight transfer function

HYDRAULIC EFFICIENCY OF A HYDROSTATIC TRANSMISSION WITH A VARIABLE DISPLACEMENT PUMP AND MOTOR

ABSTRACT

Pumps and motors are commonly connected hydraulically to create hydrostatic drives, also known as hydrostatic transmissions. A typical hydrostatic transmission consists of a variable displacement pump and a fixed displacement motor. Maximum efficiency is typically created for the system when the motor operates at maximum volumetric displacement. The objective of this research is to determine if a hydrostatic transmission with a variable displacement motor can be more efficient than one with a fixed displacement motor. A work cycle for a Caterpillar 320D excavator was created and the efficiency of the hydrostatic drive system, controlling the swing circuit, with a fixed displacement motor was compared to the efficiency with a variable displacement motor. Both multiplicative and additive uncertainty analysis were performed to determine uncertainty models that could be used to analyze the robustness of the system with feedback control applied. A PID and an H_∞ controller were designed for a position control model, as well as velocity control. It was found that while it may seem obvious to achieve maximum efficiency at maximum displacement, there are some cases where maximum efficiency is achieved at a lower displacement. It was also found that for the given work cycle, a hydrostatic transmission with a variable displacement motor can be more efficient.

Chapter 1

INTRODUCTION

1.1 Background Information

Hydraulic systems make use of fluids under pressure in order to transmit power or carry out work at a desired location where power is required. Fluid power has proven itself to be a useful medium in technology throughout history. It has been used in designs as simple as the water wheel and as complex as agricultural, aerospace, and construction equipment. Of the many methods of transmitting power such as electrical, pneumatic, and mechanical systems, fluid flow is advantageous for the following reasons:

1. Hydraulic pumps and motors, when compared to electric or gasoline motors of equal horsepower, are much smaller in size and weight than their counterparts.
2. Hydraulic hoses are very flexible, allowing the fluid lines to be routed around other machinery and power to be sent to almost any location.
3. Hydraulic systems are much more compact in size than a mechanical system capable of producing the same amount of force.
4. Speeds are easily varied for each operating condition and therefore a fixed gear ratio is not required.

The disadvantage of a hydraulic system is that its efficiency can be relatively low. "While the efficiency of a hydraulic system is much better than an electrical system, it's not as efficient as most mechanical systems" [1].

The primary component supplying power in the hydraulic system is the pump.

There are many different types of pump configurations, including gears pumps, vane pumps, and axial-piston pumps. "Axial-piston pumps are the most commonly used pumps because they exhibit high operating efficiencies (85% to 95%), are capable of operating at high pressures, and are capable of variable-displacement control" [2]. These pumps can also be categorized into two types, either fixed displacement or variable displacement. Fixed displacement pumps move the same volume of fluid with every cycle. The volume can only be changed when the speed of the pump is changed. Variable displacement pumps are capable of controlling the flow independently of the pump speed. This process is done by adjusting the component known as the swash plate. Through the use of the swash plate, the variable displacement pump is able to supply the specific amount of flow needed.

Axial-piston swash-plate type machines can be used interchangeably, with some restrictions, as either hydraulic pumps or motors. When operating as a pump, rotary power is converted into fluid power by a prime mover, typically an internal combustion engine. The pump pressurizes the system and power is generated by displacing fluid at a certain rate. When operating as a hydraulic motor, the fluid power obtained from the pump is converted back into rotating mechanical energy in the form of torque. From this similarity, pumps and motors can be classified as same machine operating in reverse modes.

Pumps and motors are commonly connected hydraulically to create hydrostatic drives, also known as hydrostatic transmissions or hydrostats, as shown in Figure 1. "By combining the two to create a drive-train, an infinite number of gear ratios can be created in both directions" [3]. A hydrostatic transmission can be formed by any combination of

variable or fixed displacement pumps and motors, as shown in Table 1. A typical hydrostatic transmission consists of a variable displacement pump and a fixed displacement motor. This is because maximum efficiency is typically achieved when the motor reaches maximum volumetric displacement. Hydrostatic transmissions are also more advantageous than a typical step transmission because they allow a "smooth, stepless change in ratio from full speed forward to full speed in reverse" [4]. By omitting the transition from one gear to another in a typical step transmission, the variable speed transmission is capable of consistently providing full power and full torque throughout the entire speed range. With a variable speed transmission, torque can always be transmitted between the motor and the load, even when the speed ratio is changed [5]. By allowing the volumetric displacement of the motor to vary, a wider range of operating conditions can be achieved.

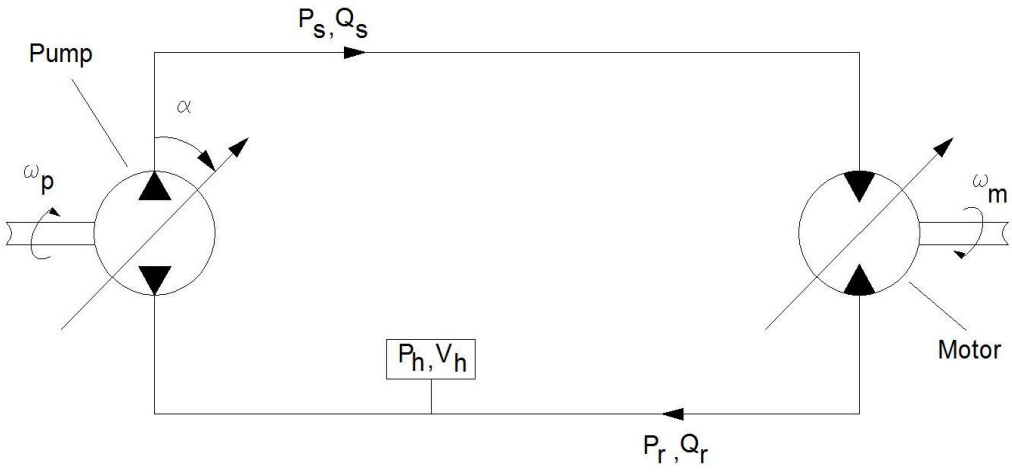

Figure 1. Hydrostatic Transmission

Table 1. Summary of Characteristics of Hydrostatic Transmission [6]

Volumetric Displacement		**Output**	
PUMP	MOTOR	TORQUE	SPEED
Fixed	Fixed	Constant	Constant
Fixed	Variable	Variable	Variable
Variable	Fixed	Constant	Variable
Variable	Variable	Variable	Variable

1.2 Pump and Motor Description

The pump is the component of the hydrostatic transmission that produces the necessary flow to the motor. The function of a variable displacement pump, as shown in Figure 3, is explained in this section. Axial-piston pumps are extensively used in hydrostatic drive systems. Axial-piston refers to the fact that the pistons are mounted parallel to the pump's x-axis, as shown in Figure 2. The general configuration consists of a certain number of evenly spaced pistons, typically nine, arranged in a circular fashion within the cylinder block assembly. The pistons, drive shaft, cylinder block, and other components form the rotating group of the pump. The swash plate is the tilted plate that is connected to the pistons by a slipper via a ball-and-socket joint. The slippers are held against the swash plate by a spring-loaded piston retainer, which is not shown in Figure 3. The swash plate is spring loaded to a maximum angle which must be overcome by the force of a servo cylinder in order lessen the angle. By controlling the pressure on the servo cylinder, the swash plate can be held at any desired angle in order to create the desired volumetric displacement. The swash plate is free to rotate about the y-axis only.

On the opposing side of the pistons, the cylinder block is pressed tightly against a valve plate by a spring. The valve plate contains two ports: 1) the intake port, which allows fluid to enter the piston chamber and 2) the discharge port, which allows the fluid to exit the piston chamber. The entire machine is contained in a fluid filled housing.

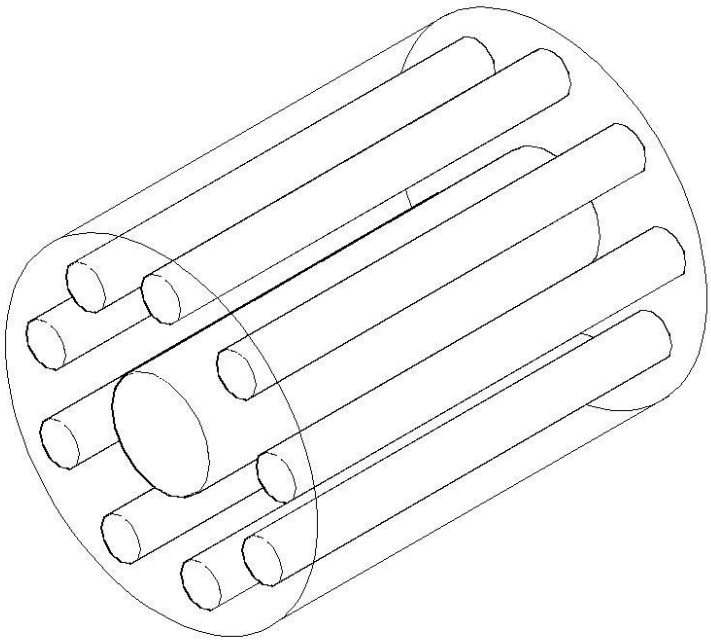

Figure 2. Axial Piston Configuration

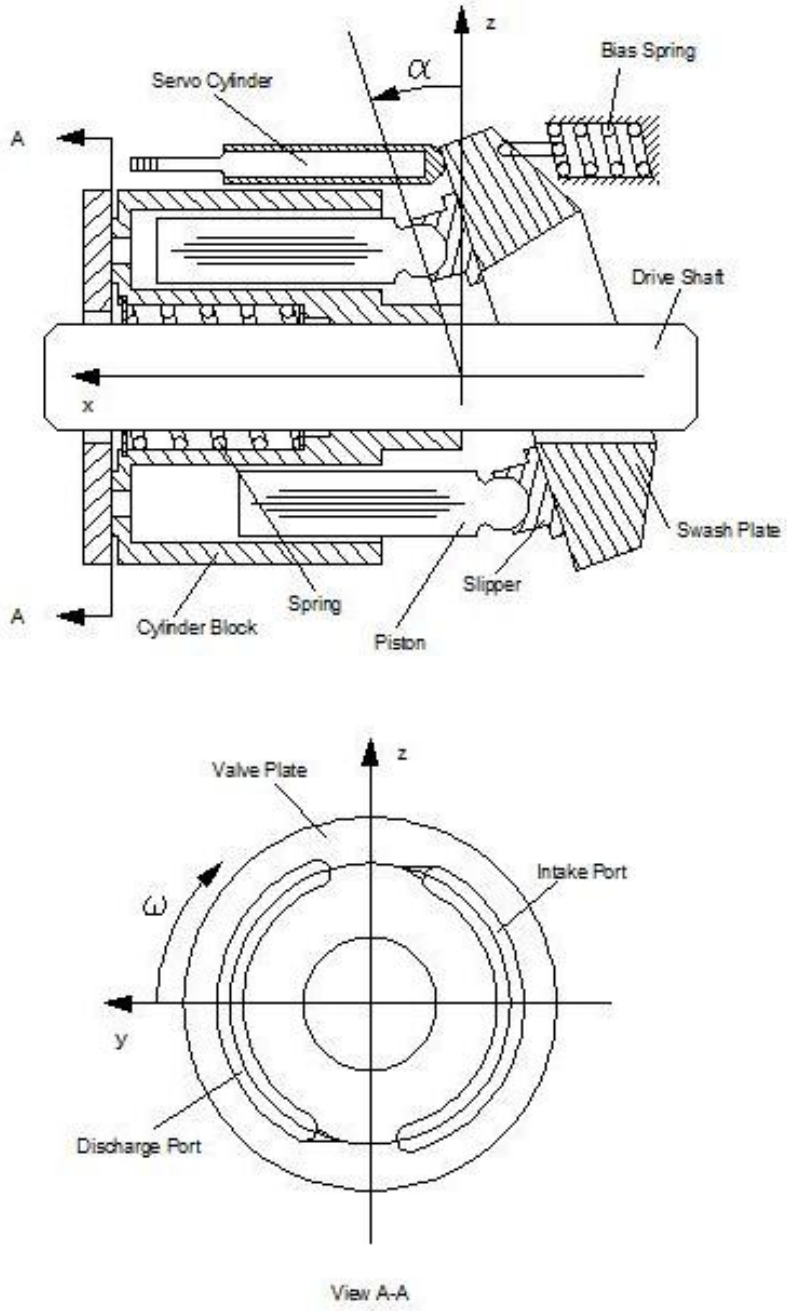

Figure 3. Variable Displacement Pump

The pump consists of two motions: 1) the rotation of the rotary group and 2) the oscillation of the pistons in and out of the cylinder block. As the input shaft turns, the pistons are pushed into the cylinder block as the slipper plates ride up the ramp of the swash plate. The pistons are pushed out of the cylinder block by the retainer as the

slippers follow the swash plate down. The pistons are aligned with the inlet and outlet ports as they are pushed out and in of the cylinder block, respectively. Fluid is drawn into the piston chamber as it withdraws from the cylinder block and passes over the intake port. Fluid is pushed out of the piston chamber as it advances into the cylinder block and passes over in discharge port. As the swash plate angle is altered, the stroke of the pistons is altered, causing the flow rate to change. When the swash plate angle is decreased, the pistons will have a shorter stroke in the block which results in a decrease in flow. When the swash plate angle is zero, there will be no movement of the pistons and therefore no flow will occur. The reciprocation of the pistons repeats itself for each revolution of the pump, thus completing the task of pumping fluid. In terms of operation, a motor is considered to be the same as a pump operating inversely.

1.3 Efficiency

Generally speaking, efficiency can be defined as the ratio of the power output by the system to the power input to the system. The purpose of a pump is to convert mechanical power into fluid power. Ideally, a pump or motor would have an efficiency of 100%, but this is not achievable because power is lost during the conversion process. The losses that occur in a pump or motor are due to friction, fluid shear, fluid compression, and leakage. The two components that make up efficiency are torque efficiency and volumetric efficiency. "Torque efficiency describes the power losses that result from fluid shear and internal friction. Volumetric efficiency describes the power losses that result from internal leakage and fluid compressibility" [2]. The overall efficiency of the unit is a product of the volumetric efficiency and the torque efficiency.

1.4 System Uncertainty

In order to evaluate the robustness of a system it is important to determine the amount of variance that exists in the system. The closed-loop (CL) control system is required to achieve a certain level of performance, stability, and the ability to withstand uncertainties within the system. A robust controller is designed to maintain stability under all expected operating conditions. Therefore, it is important to determine the operating conditions of the system. An uncertainty model is created to quantify the variance within the system. The uncertainty model is a mathematical representation, in the form of a transfer function, of the maximum error in the model. It shows the maximum variance the system will experience, as well as the robustness of the system. Nominal stability and performance are found in relation to the nominal plant (i.e. the model based on a nominal set of conditions). Once a nominal system is created, the uncertainties within the open loop (OL) system are used to find a perturbed plant (i.e. the nominal plant plus all the perturbations). The perturbed plant is then used to determine the robust stability and performance of the closed loop (CL) system. Uncertainty due to efficiency and volumetric displacement affects the CL performance of the system, therefore it is important to perform an uncertainty analysis.

1.5 Literature Review

The modeling of hydraulic pumps and motors has been addressed several times in the academic community over the past several decades. Mathematical models of performance and efficiency have been created and developed continuously. The theory of positive displacement pumps and motors, published by Wilson [7], formed the

foundation of a major component used in the fluid power industry. The basic models Wilson developed for torque and volumetric efficiencies included leakage equations, viscous torque formulas, and energy losses due to low Reynolds number flow. From this research Schlosser [8, 9] introduced terms to account for leakage at high Reynolds number flow. A more recent model, developed by Manring and Shi [10], improved the torque efficiency model based on the consideration of the lubrication conditions that exist within the pump. Models to improve efficiency and performance of hydrostatic pumps and motors have been designed and improved by the academic community on an ongoing basis.

The models created from the previous authors, with the exception of Manring and Shi [10], were considered for fixed displacement pumps only. In 1969, Thoma [11] introduced a fractional coefficient which enabled the previous models to account for a variable displacement unit. Merritt [12], who is considered an authority on hydraulic components, contributed a great deal of knowledge to the academic community, but he and Thoma [13] didn't include the dynamics associated with a swash plate type unit. Zeiger and Akers [14, 15] made their contribution by studying the dynamics of the swash-plate control for a variable displacement axial-piston pump. Since their work, more attention has been applied to the modeling of variable displacement pump, such as the work of Manring and Johnson [16].

With their growing popularity, hydrostatic transmissions have been a favored power-train for both agricultural and construction equipment "[…] because they provide a satisfactory combination of compactness, cost, and location flexibility" [5]. The fundamentals, although purely conceptual, of both hydrostatic transmissions and their

components are described in several previous works [1, 4, 6, 17]. Studies by the academic community, such as Manring and Luecke [18], have provided a better understanding of the dynamics and a more accurate model of these transmissions. The effectiveness of hydrostatic transmissions in mobile equipment has been shown in studies such as the work of Peterson, Manring, and Kluever [19]. The previous studies all involve a hydrostatic transmission with a fixed displacement motor. Some studies incorporate a hydrostatic transmission with a variable displacement motor, but the efficiency of the system is focused on regenerative braking or including an accumulator to store energy and increase efficiency [20-22].

As a modern update to Merritt's text [12], Manring [2] has addressed the fundamental concepts of fluid mechanics, systems dynamics, and control theory. An updated analysis of the axial-piston pump, pump control for swash-plate type machines, along with control objectives such as position and velocity control have also been included. With the knowledge obtained from these sources, primarily Manring [2], a model was designed in this work to investigate the efficiency and energy savings of a hydrostatic transmission with both a variable displacement pump and motor.

1.6 Objectives/Overview

The objective of this research is to determine the efficiency benefits of hydrostatic transmissions using a variable displacement pump together with a variable displacement motor. When considering the design of a hydraulic control system, sizing the motor in accordance with expected load requirements is a common starting point. The maximum pressure and working torque are then used together to design the fixed volumetric

displacement of the motor. Although a fixed displacement motor configuration is most efficient at full load, energy is wasted during any other operating condition. While it is assumed that a hydraulic motor is most efficient while operating at maximum displacement, this work demonstrates that maximum efficiency is achievable when the motor is not at the maximum possible displacement in some cases. According to Lambeck, when combining a variable displacement pump with a variable displacement motor, "The maximum motor displacement is used for maximum torque while […] the lower displacement is used for high speeds" [4]. While the cost difference between a fixed displacement and variable displacement pump is substantial, even a small increase in efficiency can provide a significant cost and energy savings over the lifetime of the pump. Therefore, it is worth investigating the use of a variable displacement motor. Finally, the efficiency and performance of a fixed displacement motor model was compared to a variable displacement motor model to control the swing circuit of a Caterpillar 320D excavator. Chapter 2 outlines the dynamic and efficiency model and its accuracy. The analysis which determines the motor displacements that result in the greatest efficiency is shown in Chapter 3. An uncertainty analysis of the hydrostatic drive system is conducted in Chapter 4, and a discussion of simulation and analytical results can be found in Chapter 5. Chapter 6 contains an overview of findings of this work, along with suggestions for future work. As a supplement to this work, a summary of the physical parameters used to create an accurate model are presented in the Appendix.

Chapter 2

MODELING THE SYSTEM

2.1 Introduction

This chapter develops the fundamental dynamic behavior that will be vital to the hydrostatic transmission modeling. This modeling also includes the necessary force analysis and hydraulic component analysis needed to accurately model the hydrostatic transmission. The hydraulic components include the pump, motor, and connecting hoses. The purpose for developing this model is to design a control system for an excavator and simulate a work cycle to check performance and efficiency.

2.2 Pump Model

The pump is the component that produces the volumetric flow necessary to supply the motor. The pump used in the hydrostatic transmission is capable of variable displacement. It is possible for this type of pump to create flow in forward, as well as reverse modes. In order to simplify the problem for this study, the pump will only be allowed to create flow in the forward direction. As previously mentioned, none of these machines are 100% efficient due to the fact that power is lost during the process of power conversion. In its most basic form, efficiency can be expressed as

$$\eta = \frac{P_{out}}{P_{in}}, \tag{2.1}$$

where P_{out} is the power output by the system and P_{in} is the power input to the system. The overall efficiency of the machine is comprised of two components, volumetric efficiency, η_v, and torque efficiency, η_t. This combination is represented by

$$\eta = \eta_v \eta_t, \tag{2.2}$$

where volumetric efficiency is expressed as

$$\eta_v = \frac{Q_d}{V_d \omega}, \tag{2.3}$$

and torque efficiency is written as

$$\eta_t = \frac{V_d P_d}{T}. \tag{2.4}$$

The use of the volumetric displacement, V_d, allows the overall efficiency to be separated so that research may be conducted by considering the discharge pressure P_d, input torque T, discharge flow Q_d, angular shaft speed ω, volumetric efficiency, or torque efficiency independently. It should be noted that due to its cancellation, the volumetric displacement has no effect on the overall efficiency.

Pump efficiency is commonly plotted against the dimensionless group $\mu\omega/P$, as shown in Figure 4, where μ is the fluid viscosity and P is the pressure drop across the pump. According to Manring, "Many attempts have been made to model pump efficiency with some degree of accuracy, […] but there does not seem to be an accurate way to predict pump efficiency characteristics, and therefore, experimental coefficients are still required in the modeling process" [2]. Adhering to Manring's statement, the volumetric and torque efficiencies can be rewritten respectively as

$$\eta_v = 1 - C_l \frac{P}{\mu\omega\alpha} - C_t \sqrt{\frac{P}{\mu\omega\alpha}}, \tag{2.5}$$

and

$$\eta_t = 1 - C_s - C_c \frac{\mu\omega}{P\alpha} - C_h \sqrt{\frac{\mu\omega}{P\alpha}}, \tag{2.6}$$

where the experimental coefficient C_l represents the fluid compressibility effects and low-Reynolds-number leakage, C_t represents high-Reynolds-number leakage, C_s represents the starting torque losses, C_c represents the Coulomb friction torque losses that are proportional to applied loads within the pump, and C_h represents the hydrodynamic torque losses that result from fluid shear. It should be noted that Manring also states that, "The determination of these coefficients is best achieved by using a least-squares evaluation with a sufficiently large number of experimental data points that have been used for determining the actual efficiencies corresponding to the dimensionless group $\mu\omega/P$" [2].

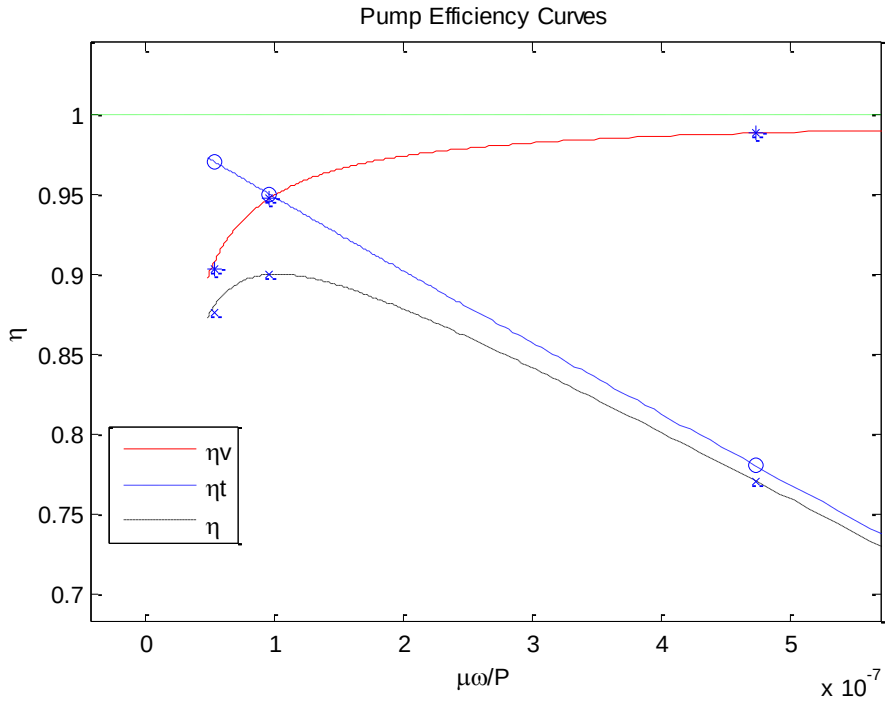

Figure 4. Typical Pump Efficiency Plot

With the pump model defined, the next component in the system needing definition is the motor.

2.3 Motor Model

The motor is the component that converts the fluid power supplied by the pump back into mechanical shaft power. The motor can be modeled by

$$J_{eq}\dot{\omega}_m + \left(b_{eq} + \frac{\eta_{t_m}}{\eta_{v_m}} \frac{D_m^2}{K} \right) \omega_m = T_m - T_{load}, \tag{2.7}$$

where J_{eq} is the equivalent moment of inertia of the rotating mass, $\dot{\omega}_m$ is the motor angular acceleration, b_{eq} is the equivalent viscous drag coefficient, D_m is the motor volumetric displacement, K is the leakage coefficient, ω_m is the motor angular velocity, T_m is the torque produced by the motor, T_{load} is the load torque exerted on the motor shaft due to a disturbance torque, and $\dot{\omega}_m$ is the angular acceleration of the motor. Pumps and motors can be classified as the same machine operating in opposite modes. So, Equation (2.2) may also be used to describe the overall motor efficiency. Since the motor operates inversely of the pump, the torque and volumetric efficiencies are respectively given by

$$\eta_t = \frac{T_{out}}{V_d P_i}, \tag{2.8}$$

and

$$\eta_v = \frac{V_d \omega}{Q_i}, \tag{2.9}$$

where V_d, is the volumetric displacement, T_{out} is the output torque on the motor shaft, ω is the angular velocity of the motor, P_i is the inlet pressure, and Q_i is the volumetric flow rate into the motor. It is important to note that the efficiency equations of the motor are

essentially the reciprocal of the efficiency equations of the pump. Since motor efficiency curves are plotted against the same dimensionless group as the pump efficiency curves, Equations (2.5) and (2.6) may be used to model the motor efficiency. Manring gives a word of caution on the subject stating, "Even though the efficiency characteristics of a motor are similar to those of a pump, the coefficients may be different. This is due to the fact that the internal parts are loaded differently when the machine is running in a pumping mode as opposed to an actuation mode. Therefore it is recommended that efficiency measurements for a machine operating as a motor be taken while the machine is functioning as an actuator and that pumping efficiencies should not be used as equivalent actuation efficiencies for the same machine" [2].

With both the pump and the motor models defined, the system of hoses connecting the two components needs to be defined. Thus, a model describing the pressure transient within the connecting hoses must be developed.

2.4 Hose Pressure Model

A system of hoses is necessary in order deliver the fluid supplied by the pump to the motor. The flow produced by the pump will create an increase in pressure in the connecting hoses. The pressure-rise rate within the hose system can be obtained from the principles of mass conservation as well as the definition of the effective fluid bulk modulus. By neglecting fluid inertia within the system, this equation can be written as

$$\dot{P}_h = \frac{\beta}{V_h} Q_h, \tag{2.10}$$

where β is the effective fluid bulk modulus, Q_h is the volumetric flow rate through the hose, and V_h is the volume of the hose. The effective fluid bulk modulus describes the elasticity of a fluid as it undergoes a volumetric deformation [2]. It can be written as

$$\frac{1}{\beta} = \frac{1}{\beta_l} + \frac{1}{\beta_a} + \frac{1}{\beta_c} \tag{2.11}$$

where β_l is the bulk modulus of the liquid, β_a is the bulk modulus of air, and β_c is the bulk modulus of the container. The liquid bulk modulus can be expressed as

$$\beta_l = K_o\left(1+\frac{(m-1)P}{K_o}\right)\left(1+\frac{mP}{K_o}\right) \tag{2.12}$$

where K_o is the secant bulk modulus of the liquid at zero gauge pressure, m is the slope of increase, and P is the pressure. The effect of air on the bulk modulus is assumed to be negligible for this work. The bulk modulus of the container can be described as

$$\frac{1}{\beta_c} = \frac{2}{E}\left(\frac{D_o^2 + d_o^2}{D_o^2 - d_o^2} + \nu\right) \tag{2.13}$$

where E is the elastic modulus of the container material, ν is Poisson's ratio, D_o is the outside diameter of the hose, and d_o is the inside diameter of the hose. The effects of leakage also need to be included in the system, therefore the volumetric flow rate through the hose system can be written as

$$Q_h = Q_p - Q_{leak} - Q_m, \tag{2.14}$$

where Q_p is the volumetric flow rate of the pump, Q_{leak} is the volumetric flow rate for leakage throughout the system, and Q_m is the volumetric flow rate of the motor. The leakage flow throughout the system can be expressed as

$$Q_{leak} = KP_h, \tag{2.15}$$

where P_h is the pressure within the hose and K is the leakage coefficient. By combining Equations (2.10) through (2.15), and noting Equations (2.3) and (2.9) the pressure-rise rate for hose assembly can be written as

$$\dot{P}_h = \frac{\beta}{V_h}\left(\frac{V_p\omega_p}{\eta_{v_p}} - KP_h - \frac{V_m\omega_m}{\eta_{v_m}}\right). \tag{2.16}$$

Many of the key variables in the system of hoses such as hose size, initial hose volume, and fluid velocity through the hose can be found from the following sources [2, 23, 24].

With all of the components defined, including the components necessary to complete the connection of the system, a model describing the overall efficiency of the system can be developed.

2.5 Efficiency Model

Since the overall efficiency of both the pump and the motor are now specified, the overall efficiency of the system can be defined. The overall efficiency of each component is still comprised of both torque and volumetric efficiencies, as shown by

$$\eta_p = \eta_{v_p}\eta_{t_p}, \tag{2.17}$$

and

$$\eta_m = \eta_{v_m}\eta_{t_m}. \tag{2.18}$$

Finally, the overall efficiency of the system can be expressed as

$$\eta = \eta_p\eta_v, \tag{2.19}$$

where η_p represents the overall pump efficiency and η_m represents the overall motor efficiency. From Equation (2.1), efficiency can also be represented in the form of energy. The energy of the system can be described by

$$E = \int P dt \tag{2.20}$$

where E is energy and P is power. Therefore, the efficiency of the system can be written as

$$\eta = \frac{E_{out}}{E_{in}} \tag{2.21}$$

where E_{out} is the energy output by the system and E_{in} is the energy input to the system.

With the entire system of the hydrostatic transmission and all of its components defined, it is now necessary to establish a model of the excavator.

2.6 Excavator Model

An excavator is a common type of off-highway equipment that uses a hydrostatic transmission. The typical work cycle of an excavator consists of two types of motion: 1) the digging and dumping of the load and 2) the rotation of the excavator between a dig site and a dump site. The excavator begins its cycle at the dig site. The bucket is lowered and filled with soil, rocks, or other debris. Next the bucket is raised and the operator rotates the excavator to the dump site, typically a stationary truck. The load is then dumped into the truck and the excavator rotates back to the dig site. The process repeats itself numerous times until the job is complete. Figure 5 illustrates the hydrostatic transmission controlling the swing circuit of the excavator. It's important to note that the pump, motor, and internal combustion engine are all located inside the

excavator housing, but shown otherwise for simplification. In order to simplify the model, reversible flow is not allowed between the pump and motor and therefore the excavator can rotate in only one direction. Instead of the excavator making a simple quarter turn back and forth, it must rotate a full 360 degrees back to the dig site. The motor velocity and load torque for the work cycle proposed in this work can be seen in Figure 6 and Figure 7.

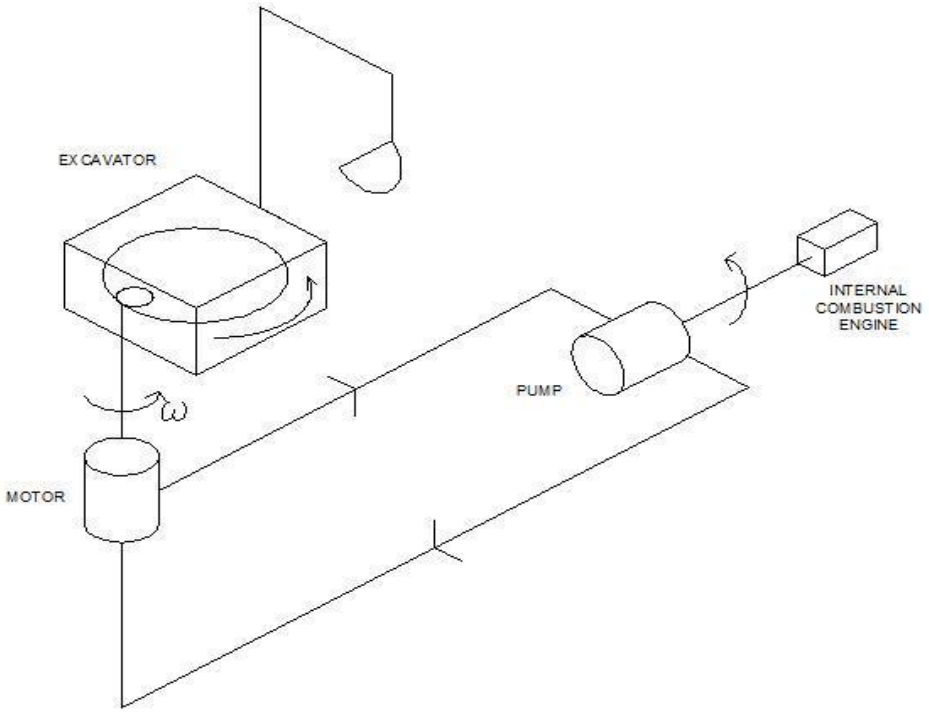

Figure 5. Swing Circuit Diagram

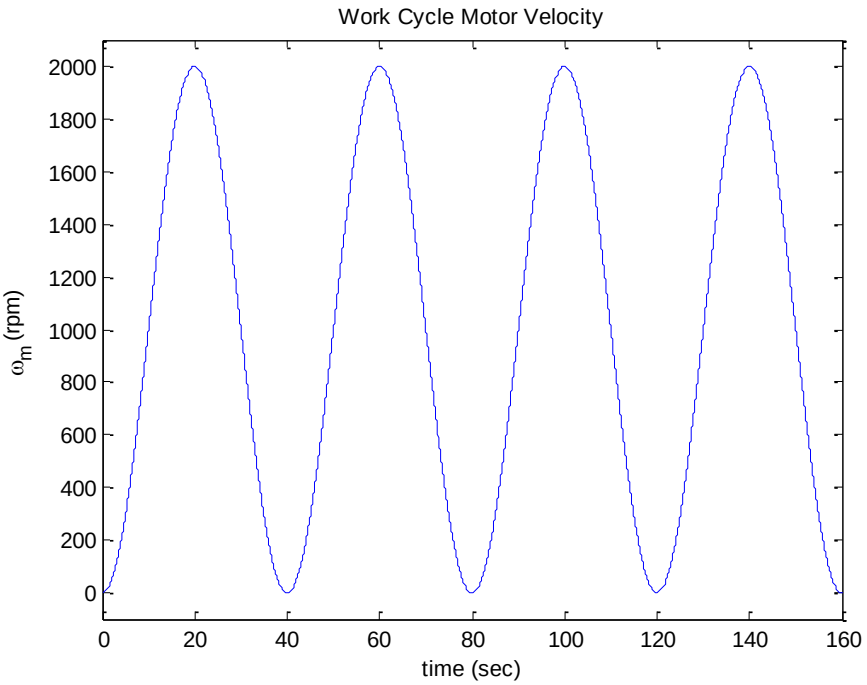

Figure 6. Work Cycle Motor Velocity

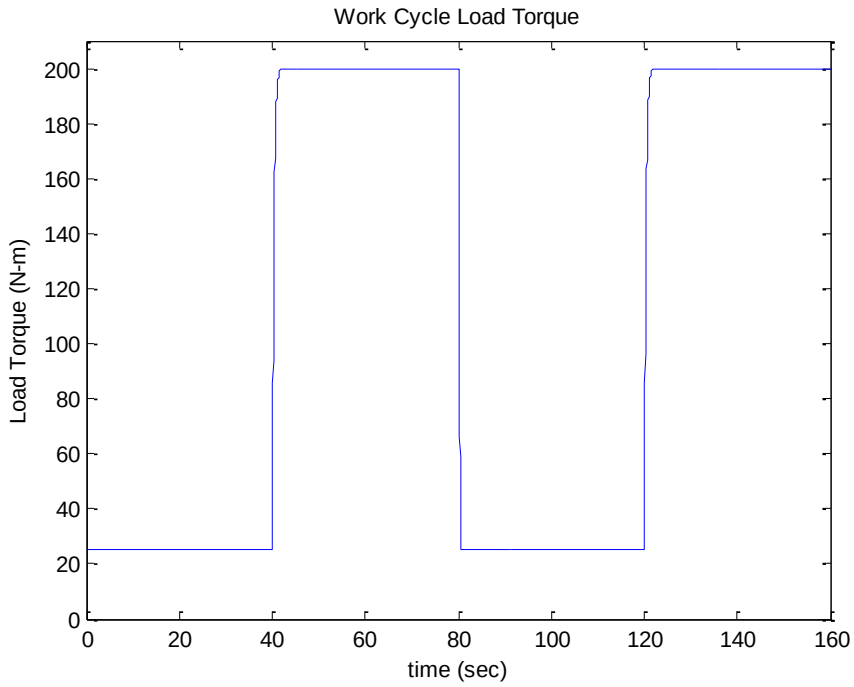

Figure 7. Work Cycle Load Torque

Multiple models of a Caterpillar 320D excavator were created based on literature published by Caterpillar [25]. The primary model is a linear, fixed displacement motor model proposed by Manring [2]. The model can be expressed by

$$J_{eq}\dot{\omega}_m + \left(b_{eq} + \frac{\eta_{t_m}}{\eta_{v_m}} \frac{D_m^2}{K} \right) \omega_m = \frac{\eta_{t_m} \eta_{v_p} D_m D_p \omega_p}{K \alpha_{\max}} \alpha - T_{load}, \tag{2.22}$$

where D_p is the pump volumetric displacement, α is the swash plate angle, and α_{max} is the maximum swash plate angle. This model assumes that the pressure transients associated with the connecting hoses are negligible, as well as a fixed pump input speed and maximum pump volumetric displacement. The parameters that may vary include the motor volumetric displacement, efficiency, speed, and load torque. Each of these varying parameters have limitations on their minimum and maximum values. A free-body diagram of the excavator containing the forces acting on it is shown in Figure 8Figure 8.

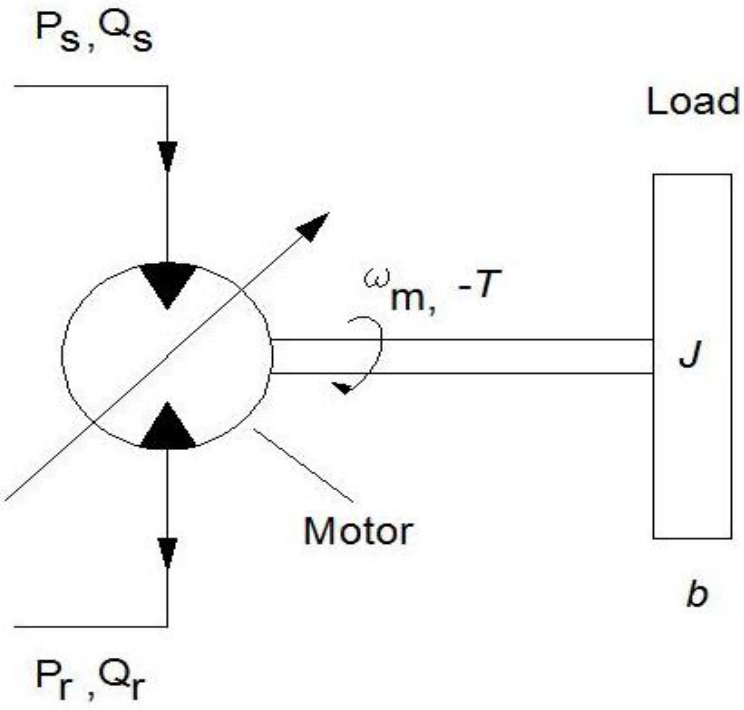

Figure 8. Excavator Free-Body Diagram

Since the motor will need to produce the greatest amount of torque and volumetric displacement when the bucket is full, the hydrostatic transmission is typically configured to produce the greatest efficiency during the fully loaded phase of the work cycle. For this reason, an emphasis will be placed on increasing efficiency during the low load phases of the work cycle when the bucket is empty. Using the previously mentioned models, Simulink® models representing the excavator with a fixed displacement motor and a variable displacement motor were created, and are shown in Figure 10 and Figure 10, respectively.

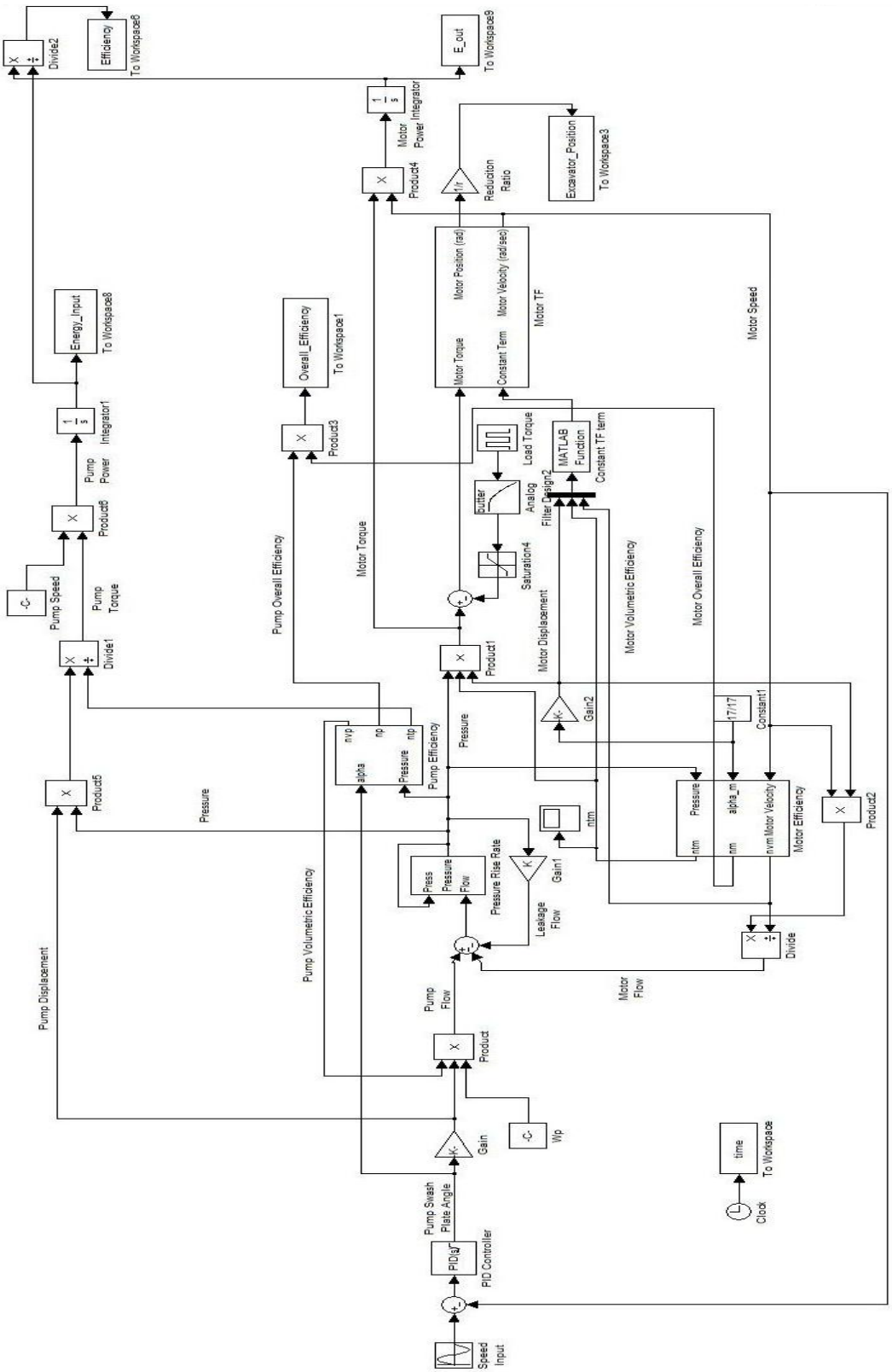

Figure 9. Fixed Displacement Motor Model

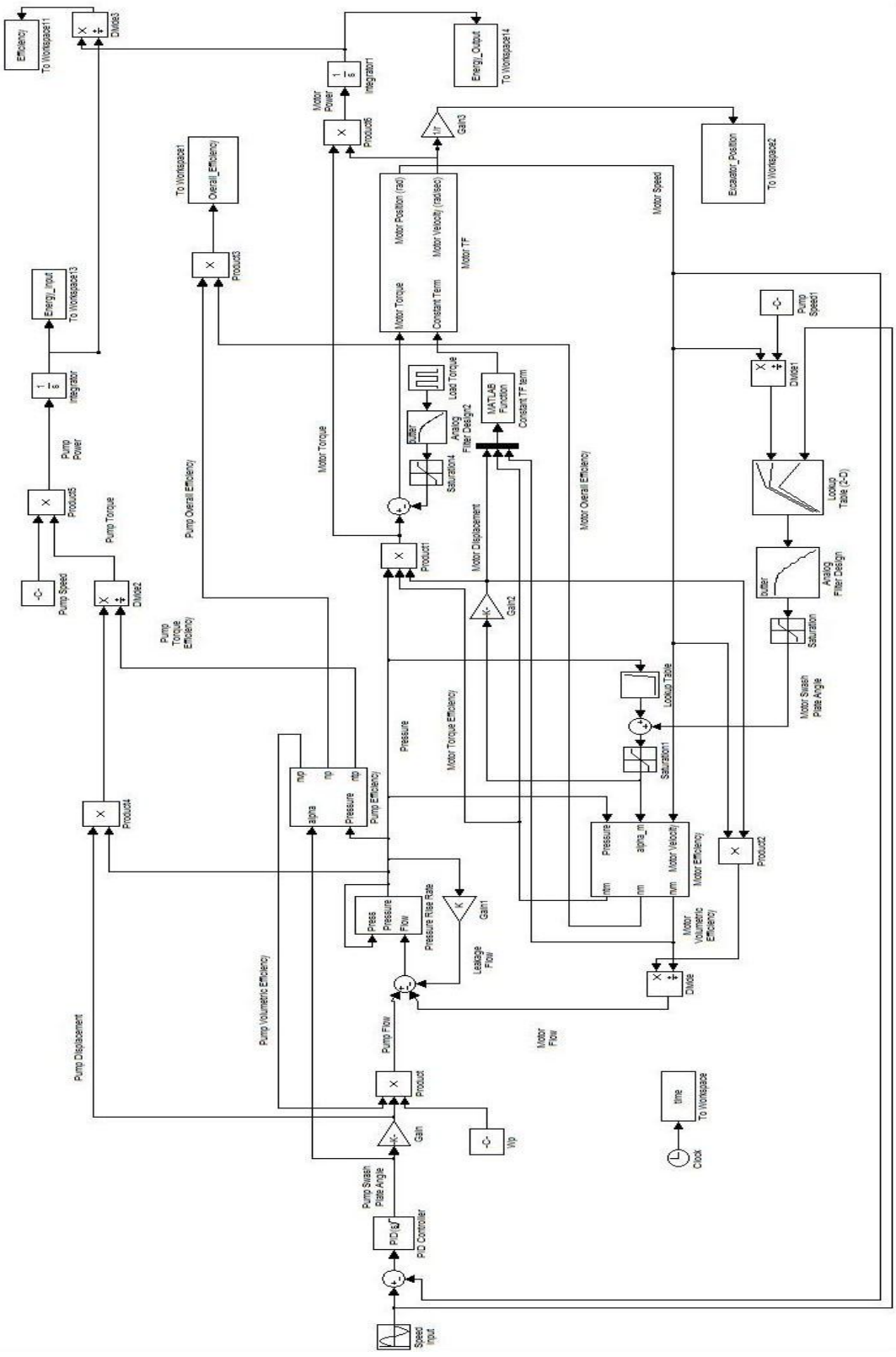

Figure 10. Variable Displacement Motor Model

2.7 Control Models

Two types of control systems were used in this work, position (point-to-point) control and velocity control. The primary control objective of the position control model is the ability to position the load accurately at a specified location. This control type is commonly referred to as "dig-to-dump". Position control allows the machine to move accurately to predefined locations, but sacrifices the speed control and is typically carried out under slow moving conditions. A more common control objective is angular velocity control. This objective attempts to produce a specified output angular velocity for the load based on a desired angular velocity. Velocity control is advantageous because it can also be used by an operator to control position, but the position controlled system can become unstable due to the presence of the additional integrator in the transfer function. Position and velocity control models are shown in Figure 12 and Figure 12, respectively. These types of control methods will be applied to the excavator model in a later chapter. Typically, most machines use open loop control in an attempt to achieve a desired performance requirement, while ultimately giving the operator control of the equipment. The disadvantage of open loop control is its inability to affect the performance of the system due to the fact that no electronic feedback is sent to reduce error. The reasoning for considering a closed loop system is the ability to achieve maximum performance of the system.

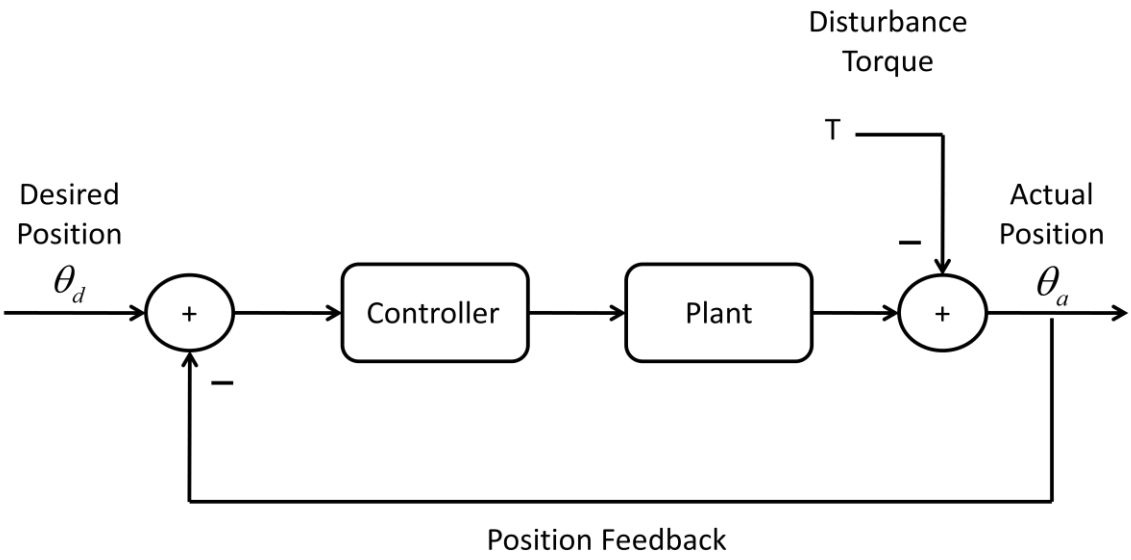

Figure 11. Position Control Model

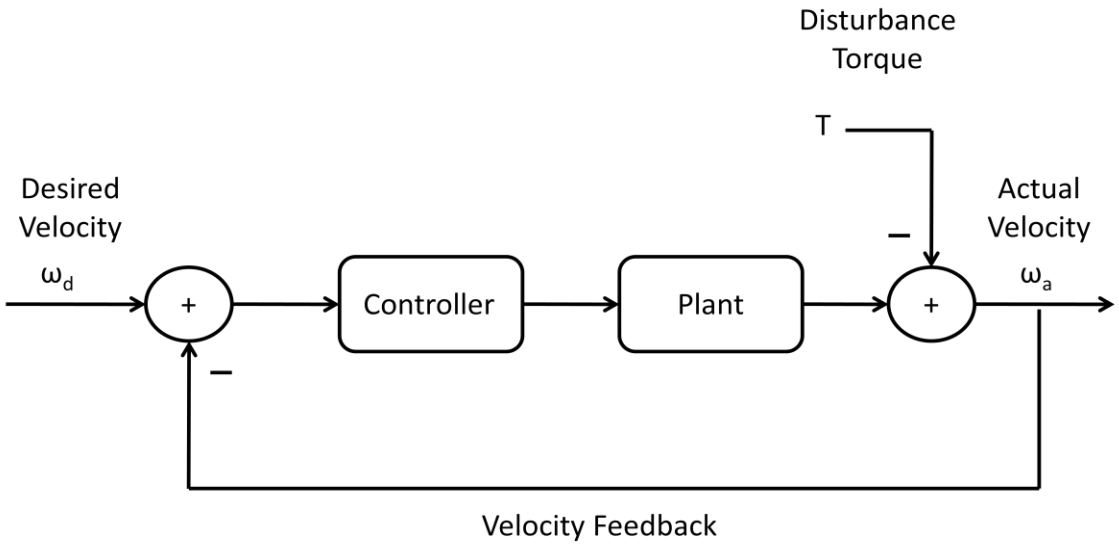

Figure 12. Velocity Control Model

2.8 Conclusion

This chapter describes the development of a mathematical model that accurately represents a hydrostatic transmission. In particular, the equations describing volumetric and torque efficiencies are presented, as well as the overall efficiency of the system and

the pressure transient within the system. Finally, a model of an excavator and its typical work cycle was presented, along with two types of control. Next, an analysis using the models developed in this chapter must be performed in order to find cases when the maximum overall efficiency is achieved. This topic will be discussed in the following chapter.

Chapter 3

ANALYSIS

3.1 Introduction

The previously described system model can be utilized to perform an optimization of the motor volumetric displacement. This requires solving for the experimental coefficients noted in the previous chapter, determining the appropriate pressure, and finding the optimal motor displacement for the hydrostatic transmission. Adjustments also need to be made to the oil temperature, speed ratio, and output torque in order to determine the optimal motor displacement. The optimization method, uncertainty analysis, and excavator model analysis developed from the models presented in Chapter 2 will be described in this chapter.

3.2 Solving for coefficients

The pump efficiency model defined by Equations (2.5) and (2.6) contains the terms C_l, C_t, C_s, C_c, and C_h which must be determined from experiments. Since no actual experiment was conducted in this work, experimental results were obtained from Manring [26]. The experimentally obtained efficiency results were presented in six separate figures: pump torque efficiency, motor torque efficiency, pump volumetric efficiency, motor volumetric efficiency, pump overall efficiency, and motor overall efficiency. Three points were selected from each torque and volumetric efficiency curve, as shown by the markers in Figure 14 and Figure 14. The parameters obtained from the conditions of the experimental results were swash plate angle, pressure, angular velocity,

viscosity, and efficiency. With the all the necessary parameters defined, a set of simultaneous equations was created from Equations (2.5) and (2.6) shown by

$$\begin{Bmatrix} \eta_{v_1} - 1 \\ \eta_{t_1} - 1 \\ \eta_{v_2} - 1 \\ \eta_{t_2} - 1 \\ \eta_{v_3} - 1 \end{Bmatrix} = \begin{bmatrix} -\frac{P_1}{\mu\omega\frac{\alpha}{\alpha_{\max}}} & -\sqrt{\frac{P_1}{\mu\omega\frac{\alpha}{\alpha_{\max}}}} & 0 & 0 & 0 \\ 0 & 0 & -1 & -\frac{\mu\omega}{P_1\frac{\alpha}{\alpha_{\max}}} & -\sqrt{\frac{\mu\omega}{P_1\frac{\alpha}{\alpha_{\max}}}} \\ -\frac{P_2}{\mu\omega\frac{\alpha}{\alpha_{\max}}} & -\sqrt{\frac{P_2}{\mu\omega\frac{\alpha}{\alpha_{\max}}}} & 0 & 0 & 0 \\ 0 & 0 & -1 & -\frac{\mu\omega}{P_2\frac{\alpha}{\alpha_{\max}}} & -\sqrt{\frac{\mu\omega}{P_2\frac{\alpha}{\alpha_{\max}}}} \\ 0 & 0 & -1 & -\frac{\mu\omega}{P_3\frac{\alpha}{\alpha_{\max}}} & -\sqrt{\frac{\mu\omega}{P_3\frac{\alpha}{\alpha_{\max}}}} \end{bmatrix} \begin{Bmatrix} C_l \\ C_t \\ C_s \\ C_c \\ C_h \end{Bmatrix}. \qquad (3.1)$$

Finally, left division was performed, using the MATLAB® command *mldivide*, in order to solve for the unknown experimental coefficients. This command determines the solution using a least squares method. A set of coefficients obtained from experimental data were found for both the pump and motor efficiency models.

3.3 Pump and Motor Plots

With the pump and motor coefficients determined, their accuracy must be verified. In order to verify the accuracy of the coefficients, the efficiency curves which the coefficients were calculated from must be replicated. As mentioned previously by Manring, the pumping coefficients should not be used as equivalent motor coefficients. This statement was verified by an attempt to use the pump coefficients also as the motor coefficients. As a result, the pump efficiency model was accurately replicated, but the motor efficiency model failed to produce identical results. When the motor coefficients were used in the motor efficiency model, the original experimental data was successfully

duplicated. Based upon these results, it was proven that the experimental coefficients were calculated correctly and is shown in Figure 14 and Figure 14.

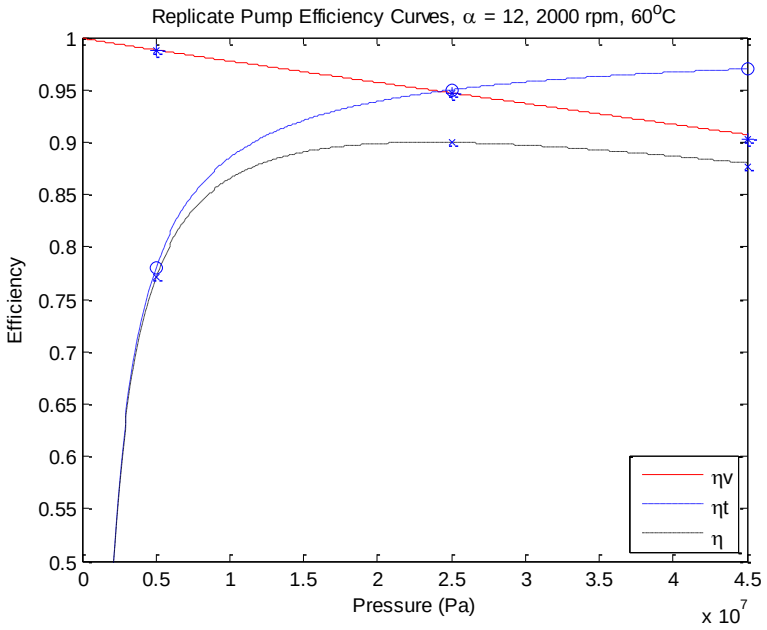

Figure 13. Pump Efficiency Curves

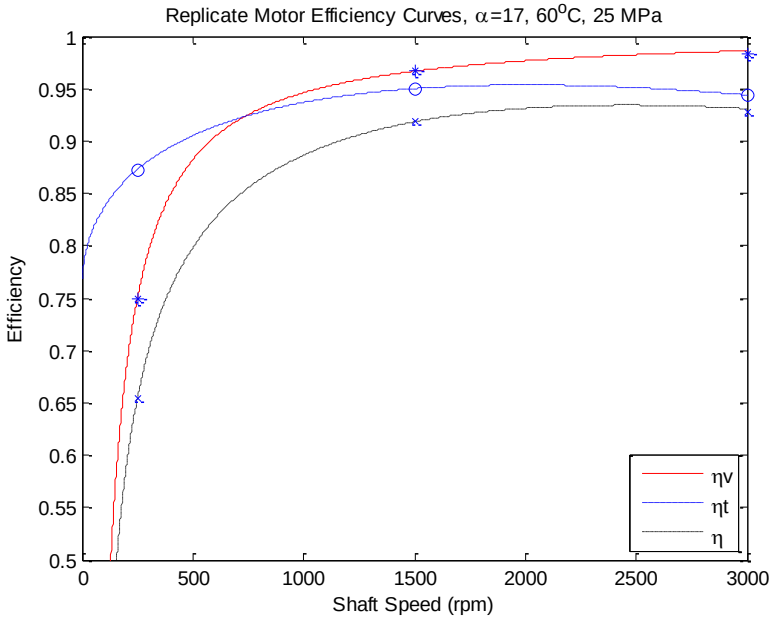

Figure 14. Motor Efficiency Curves

3.4 Optimization

In order to determine the optimal motor displacement capable of producing the greatest overall efficiency, an optimization method was performed using MATLAB®. First, a speed ratio between the pump and motor, oil temperature, and desired output torque was determined. Then a range of volumetric displacements for the motor was chosen, specifically 1-140 cm^3/rev. The following procedure was performed for each motor volumetric displacement in the loop. Pressure was determined using the MATLAB® function *fminsearch.m* and setting the motor torque efficiency from Equations (2.6) and (2.8) equal to zero. This is shown by

$$\left(1-C_s-C_c\frac{\mu\omega}{P\alpha}-C_h\sqrt{\frac{\mu\omega}{P\alpha}}\right)-\left(\frac{T_{out}}{D_mP}\right)=0, \tag{3.2}$$

Using the results from this optimization method, the motor torque and volumetric efficiencies were determined. Next, the MATLAB® function *fminbnd.m* was used to determine the swash plate angle of the pump by employing the volumetric efficiency from Equation (2.5) and setting the flow of the pump and motor from Equations (2.3) and (2.9) equal to each other. This is represented by

$$\left(1-C_l\frac{P}{\mu\omega\alpha}-C_t\sqrt{\frac{P}{\mu\omega\alpha}}\right)D_p\omega_p=\frac{D_m\omega_m}{\eta_{v_m}}. \tag{3.3}$$

From this optimization method, the pump torque and volumetric efficiencies were determined. Next, the overall efficiencies for the pump and motor were determined and then used to calculate the overall efficiency of the system. Finally, motor volumetric displacement was compared to overall efficiency to determine the optimal displacement resulting in the greatest efficiency.

3.5 Oil, Speed Ratio, and Torque Adjustments

In an attempt to produce the optimal parameters to achieve the greatest overall efficiency at a lower motor displacement, adjustments were made to the hydraulic fluid and speed ratio between the pump and motor. Considering that it is neither desirable nor possible for the operator to control the excavator at a constant speed, different speed ratios between the pump and motor were investigated. The speed ratio between the pump and motor is represented by

$$r = \frac{\omega_m}{\omega_p} \tag{3.4}$$

where ω_m is the angular velocity of the motor and ω_p is the angular velocity of the pump The speed ratios used in this analysis are presented in Table 2. Adjustments were also made to the fluid viscosity by increasing and decreasing the temperature of the hydraulic fluid. The 10W oil temperatures ranged from 5˚C to 90˚C. Finally, adjustments were made to the output torque of the system. During a typical work cycle, the torque required to rotate the excavator between the dig site and the dump site will vary due to the load. For this reason, the previously mentioned analysis was performed for output torques ranging from 10 to 400 N-m.

Table 2. Pump and Motor Speed Ratios

Pump Speed (rpm)	Motor Speed (rpm)	Speed Ratio
2000	500	0.25
2000	1000	0.5
2000	1500	0.75
2000	2000	1

3.6 Excavator Model Analysis

Multiple excavator models were created in this analysis. Each model was a combination of a linear, nonlinear, open loop, closed loop, fixed displacement motor, and variable displacement motor models. First, a simple linear OL model with a fixed displacement motor was created. Variables including mass, boom length, maximum pressure, maximum flow, swing torque, and swing speed were listed in the Caterpillar 320D excavator catalog, but key parameters such as leakage, inertia, damping, and gear reduction ratio were missing [25]. The unknown model parameters were adjusted until the model produced results that closely match the specifications listed by Caterpillar, primarily swing speed. Next, the model was transformed into a CL nonlinear model including a pressure transient and a controller. The same process was used to create a CL, variable displacement motor model. Nonlinearities such as the pressure transient, motor swash plate angle, and motor velocity were added to the plant. The results from the optimization method previously described in Section 3.4 (which will be explained in a later chapter) were used to create a look-up table that can determine the optimal motor displacement based on motor speed and torque. The nonlinear CL fixed displacement motor and variable displacement motor models were put through an identical work cycle and overall efficiency was compared. The results will be discussed in a later chapter. For each speed ratio listed in Table 2, the optimization method was performed for a range of motor output torques from 10 to 400 N-m. Efficiency was plotted against motor swash plate angle, and the maximum overall efficiencies and corresponding swash plate angles were determined. This look-up table optimizes performance by adjusting the swash plate

angle to its optimal position based on speed ratio and torque, therefore creating the greatest overall efficiency for the system. The look-up table is shown in Table 3.

Table 3. Optimal Motor Swash Plate Look-up Table

	Torque (N-m)											
Speed Ratio $\frac{\omega_m}{\omega_p}$		10	25	50	100	150	200	250	300	350	400	$\frac{\alpha_m}{\alpha_{max}}$
	0.25	.07857	.1071	.1714	.4643	1	1	1	1	1	1	
	0.5	.1071	.1646	.9143	1	1	1	1	1	1	1	
	0.75	.9	.9571	.9929	1	1	1	1	1	1	1	
	1	.9929	.9929	.9857	.9857	.9786	.9786	.9714	.9643	.9643	.9571	

3.7 Conclusion

This chapter describes the development of a method for determining the optimal motor displacement. In order to develop this method, first unknown experimental coefficients were defined. Then, with the experimental coefficients defined, the pressure and efficiencies were calculated. With this information, the optimal motor displacement was determined for a specific speed ratio and output torque. The next step will be to develop an H_∞ controller capable meeting the desired stability and performance requirements for both additive and multiplicative uncertainty. A PID controller also needs to be developed in order to compare to the H_∞ for both the position and velocity control models.

Chapter 4

CONTROL DESIGN

4.1 Introduction

The previously modeled Caterpillar 320D utilizes a hydrostatic transmission. The motor velocity or the position of the excavator is be maintained by a controller, rather an operator, in order to achieve a higher level of performance and a faster response. This controller must achieve the desired position or velocity while sustaining a stable system and meeting performance requirements. To accomplish these requirements, both a proportional-integral-derivative (PID) and an H_∞ controller will be utilized. The "controller compares the actual value of the plant output with the desired value, determines the deviation, and produces a control signal that will reduce the deviation to zero or a small value" [27]. An uncertainty model allows for variance within the system to be quantified and allows the robustness of the system to be evaluated. Both additive and multiplicative error models are developed based on the ranges of the varying parameters. According to Skogestad and Postlethwaite, "A control system is robust if it is insensitive to differences between the actual system and the model of the system which was used to design the controller" [28]. The goal of the robust controller optimization is to develop an H_∞ controller, K_{Hinf}, such that the H_∞ norm between the inputs and outputs is less than one. This makes certain that the control system is robust to uncertainty within the system and that the performance requirements are met. Control problems, with the goal of minimizing the infinity norm, are termed H_∞ optimization problems. An H_∞ controller minimizes the worst-case gain of the system. The infinity norm refers to the

worst-case gain of the system, while the *H* term refers to the "Hardy space" [28]. A PID controller, K_{PID}, also needs to be developed in order to compare to the H_∞ controller. The performance requirements, uncertainty models, and controller design methods are presented in this chapter.

The basic requirement of CL control systems is to achieve a certain level of performance while tolerating uncertainties within the system. The control system must be robust enough to perform under conditions with large variations in parameters and unknown disturbances. To determine the stability and performance of the control system, the uncertainties within the system must first be defined. In this study, the controller must be able to adjust for variations in efficiency and volumetric displacement due to unknown torque disturbances.

4.2 Error Modeling

An important step in robust control design is to create a model of plant uncertainty using a set of parameter variations for a known range of operating conditions. For this study, a comparison will be given for two types of uncertainty models that account for perturbations in the system parameters. As previously mentioned, the two types of error models used are additive uncertainty, i.e. absolute error, and multiplicative uncertainty, i.e. relative error. Block diagrams showing multiplicative error and additive error can be seen in Figure 16 and Figure 16, respectively. The multiplicative uncertainty error and additive uncertainty error models and their transfer function weights are defined by the following relationships

$$l_I(\omega) = \max_{G_{pert} \in \Pi} \left| \frac{G_{pert}(j\omega) - G_{nom}(j\omega)}{G_{nom}(j\omega)} \right|, \tag{4.1}$$

$$\left|w_I(j\omega)\right| \geq l_I(\omega), \forall \omega, \tag{4.2}$$

$$l_A(\omega) = \max_{G_{pert} \in \Pi} \left|G_{pert}(j\omega) - G_{nom}(j\omega)\right|, \tag{4.3}$$

and

$$\left|w_A(j\omega)\right| \geq l_A(\omega), \forall \omega, \tag{4.4}$$

where $G_{pert}(j\omega)$ represents each perturbed plant from the nominal plant $G_{nom}(j\omega)$. The frequency dependent multiplicative model error magnitude, $l_I(\omega)$, is the magnitude of the difference between the frequency response of a perturbed plant and the nominal plant divided by the nominal plant. The frequency dependent additive model error magnitude, $l_A(\omega)$, is the magnitude of the difference between the frequency response of a perturbed plant and the nominal plant. As defined in Equations (4.2) and (4.4), the magnitude of w_I and w_A must be greater than or equal to l_I and l_A over all frequencies, respectively. In other words, the magnitude of the uncertainty weight bounds the maximum error (worst case scenario) for all frequencies and all possible perturbations. The MATLAB® function *fitmag.m*, which fits a stable minimum phase transfer function to magnitude data, was used in finding the 3rd-order transfer functions $w_I(s)$ and $w_A(s)$. The bounding transfer functions can be seen in Table 4 and shown in Figure 17 - Figure 20.

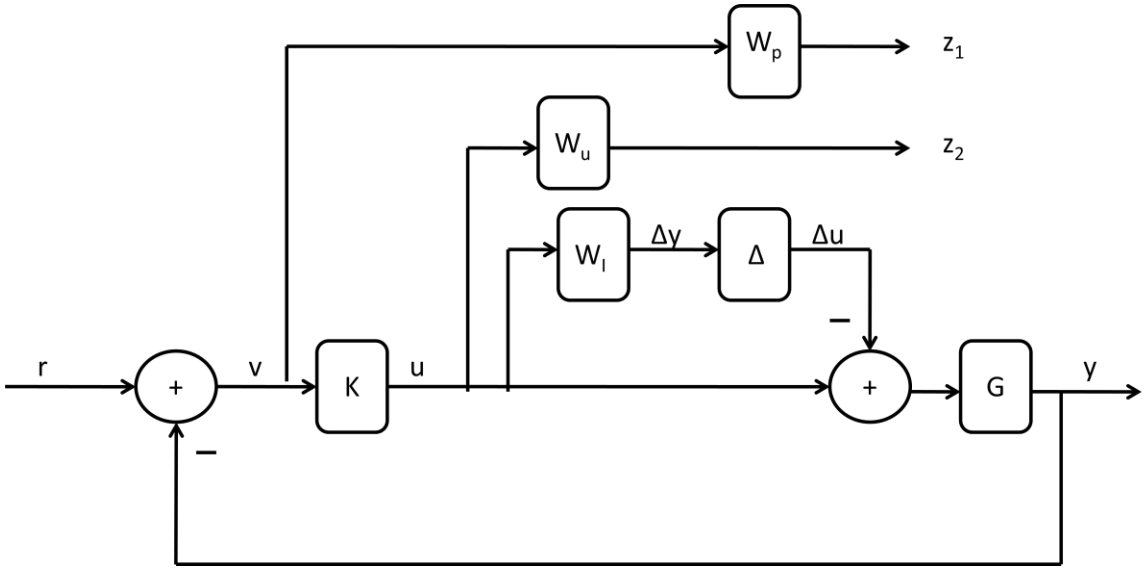

Figure 15. Closed loop control system with the multiplicative uncertainty model and performance weights

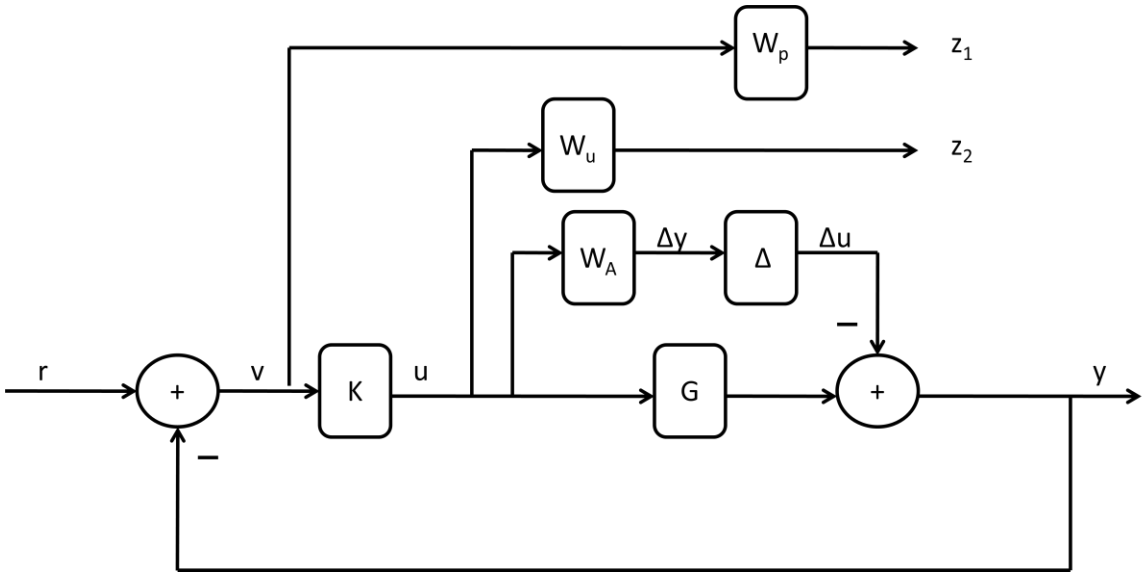

Figure 16. Closed loop control system with the additive uncertainty model and performance weights

Table 4. Bounding Transfer Functions

Uncertainty	Bounding Transfer Function	Control
Multiplicative	$w_I = \frac{0.1133s^3 + 1.102s^2 + 5.074s + 11.91}{s^3 + 12.68s^2 + 63.04s + 159.4}$	Velocity
Additive	$w_A = \frac{0.0001845s^3 + 8.402s^2 + 40.71s + 198.8}{s^3 + 13.9s^2 + 74.02s + 216.8}$	Velocity
Multiplicative	$w_I = \frac{0.1507s^3 + 14.19s^2 + 110s + 275.3}{s^3 + 96.48s^2 + 892.6s + 2326}$	Position
Additive	$w_A = \frac{0.004587s^3 + 1.426s^2 + 0.0179s + 5.043e-5}{s^3 + 0.01618s^2 + 0.0001397s + 1.274e-7}$	Position

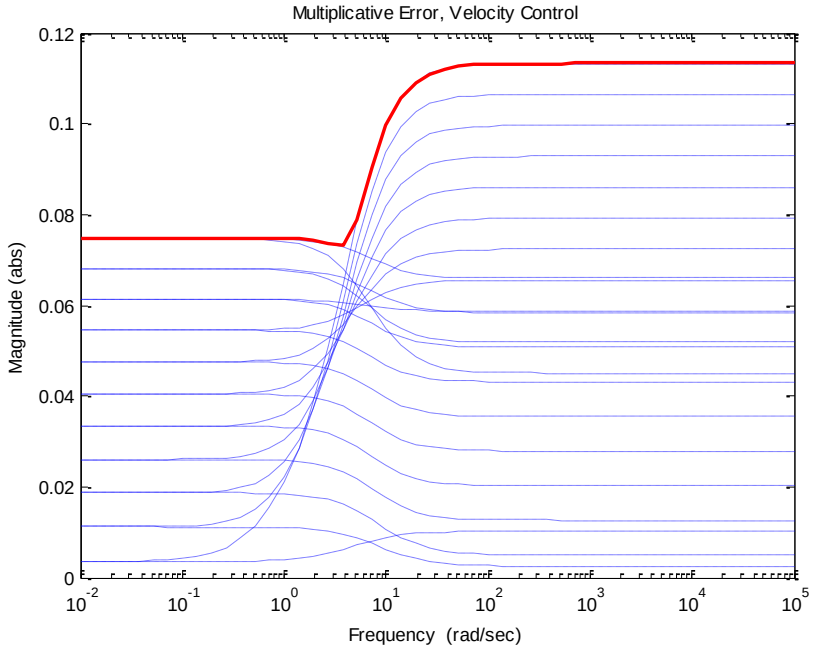

Figure 17. Multiplicative uncertainty TF bounding the maximum error, velocity control

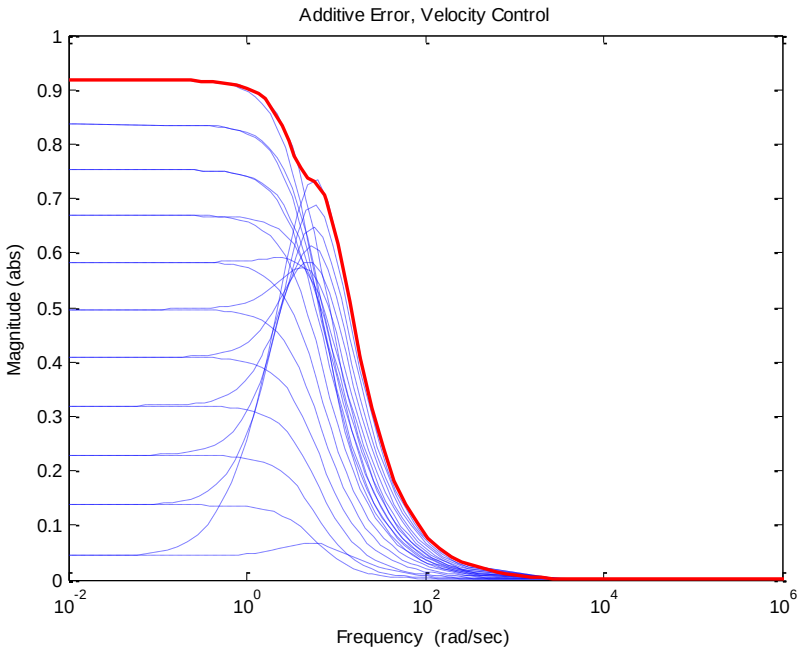

Figure 18. Additive uncertainty TF bounding the maximum error, velocity control

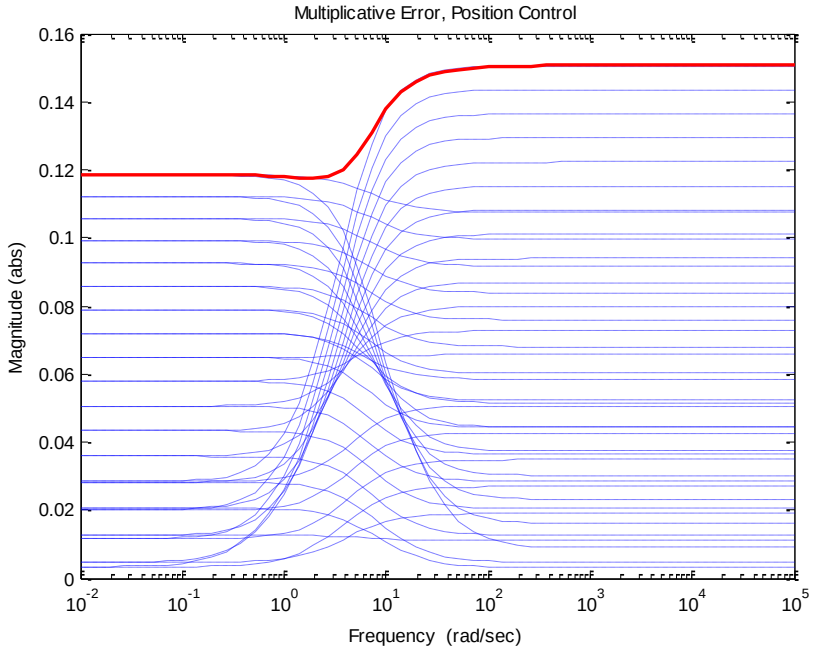

Figure 19. Multiplicative uncertainty TF bounding the maximum error, position control

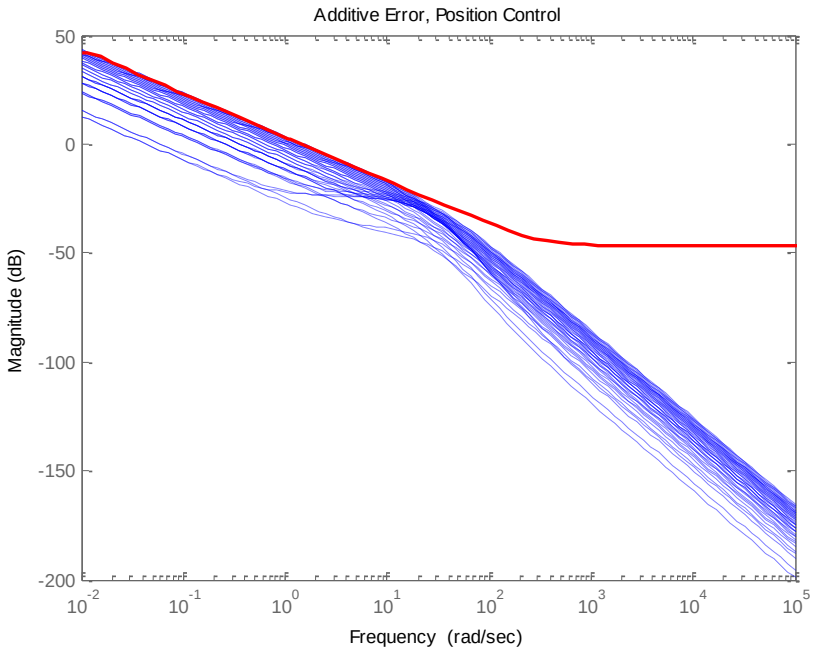

Figure 20. Additive uncertainty TF bounding the maximum error, position control

4.3 Performance

In order to analyze the performance of the system, a performance weight transfer function, $w_P(s)$, is needed. The performance weight is written as

$$w_P(s) = \frac{s/M + \omega_B}{s + \omega_B A} \tag{4.5}$$

where M is the allowable error at high frequencies, A is the allowable error at lower frequencies, and ω_B is the bandwidth frequency in hertz. M corresponds to the transient error, while A corresponds to the steady-state tracking error. The bandwidth corresponds to the crossover point between low and high frequency error. In order to meet the desired performance requirements, two performance weights were created. The first performance weight created is for design, $w_{Pdesign}$, and the second performance weight created is for analysis, $w_{Panalysis}$. A system with a larger bandwidth has better performance due to a

faster response, while a system with a smaller bandwidth has a slower response time but is usually more robust [28]. A high bandwidth for design produces a controller that yields a high bandwidth. Since the H_∞ optimization process generates a controller capable of satisfying the design specifications for the worst case scenario, it often results with a less than optimal controller. By setting the performance requirements higher during the design phase, it allows the controller to meet the desired performance following the design process and therefore have a higher chance at success. For this reason, a higher bandwidth, along with smaller high and low frequency errors, was chosen for the design performance weight. This performance weight was used in the controller design, while a performance weight with a smaller bandwidth and larger frequency errors was used for analysis. A list of the performance weights used can be seen in Table 5.

Table 5. Performance Weights

Uncertainty	$w_{Pdesign}$			$w_{Panalysis}$			**Control**
	ω_B (Hertz)	M	A	ω_B (Hertz)	M	A	
Multiplicative and Additive	3	2	0.01	1	3	0.1	Velocity and Position

The inverse of w_P represents the upper bound of the magnitude of the sensitivity function, S. The sensitivity function is the closed-loop transfer function from the output disturbances to the outputs and also the transfer function from the reference input to the tracking error output [28]. The sensitivity transfer function is represented as

$$S = \frac{1}{1 + G_{pert} K}. \tag{4.6}$$

In order for the system to meet the performance requirements defined by w_P, the H_∞ norm of the weighted sensitivity, $w_P S$, must be less than one. Alternatively, the magnitude of the sensitivity function, $|S|$, must be less than one for all frequencies. This can be expressed respectively by

$$\left\| w_P S \right\|_\infty < 1 \tag{4.7}$$

or

$$\left| S(j\omega) \right| < \frac{1}{\left| w_P(j\omega) \right|}, \forall \omega. \tag{4.8}$$

Another performance weight was added onto the control signal to limit its maximum value during the design process. The controller weight, $w_u(s)$, is used in order to limit the swash plate from reaching its maximum angle. The controller weight was set at 1/12 so the maximum control signal possible is 12˚.

4.4 Obtaining P and N Matrixes

The block diagrams in Figure 15 and Figure 16 can now be analyzed and transformed into the generalized plant *P*. The generalized plant for system with multiplicative error is

$$\begin{Bmatrix} y_\Delta \\ z \\ v \end{Bmatrix} = \begin{bmatrix} P_{11} & P_{12} \\ P_{21} & P_{22} \end{bmatrix} \begin{Bmatrix} u_\Delta \\ r \\ u \end{Bmatrix}$$
$$P_{11} = \begin{bmatrix} 0 & 0 \\ -w_P G_{nom} & w_P \\ 0 & 0 \end{bmatrix}$$
$$P_{12} = \begin{bmatrix} w_I \\ -w_P G_{nom} \\ w_u \end{bmatrix} \tag{4.9}$$
$$P_{21} = \begin{bmatrix} -G_{nom} & 1 \end{bmatrix}$$
$$P_{22} = \begin{bmatrix} -G_{nom} \end{bmatrix}$$
$$z = \begin{bmatrix} z_1 & z_2 \end{bmatrix}^T$$

where G_{nom} is the nominal plant transfer function, w_P is the performance weight, w_u is the controller weight, w_I is the multiplicative uncertainty transfer function, the output z_1 is connected to the error signal, and the output z_2 is connected to the control signal. Similarly, the generalized plant for the system with additive error is

$$\begin{Bmatrix} y_\Delta \\ z \\ v \end{Bmatrix} = \begin{bmatrix} P_{11} & P_{12} \\ P_{21} & P_{22} \end{bmatrix} \begin{Bmatrix} u_\Delta \\ r \\ u \end{Bmatrix}$$
$$P_{11} = \begin{bmatrix} 0 & 0 \\ -w_P & w_P \\ 0 & 0 \end{bmatrix}$$
$$P_{12} = \begin{bmatrix} w_A \\ -w_P G_{nom} \\ w_u \end{bmatrix} \tag{4.10}$$
$$P_{21} = \begin{bmatrix} -1 & 1 \end{bmatrix}$$
$$P_{22} = \begin{bmatrix} -G_{nom} \end{bmatrix}$$
$$z = \begin{bmatrix} z_1 & z_2 \end{bmatrix}^T$$

where w_A is the additive uncertainty transfer function. A generalized plant is formed for

each set of varying parameters and the performance weight w_P is substituted with $w_{Pdesign}$ or $w_{Panalysis}$ depending on whether the controller is designed or the uncertainty analysis is performed. It should be noted that for position control, the additional integrator resulted in a pole on the $j\omega$-axis. This caused instability, so a constant of 0.001 was added to the nominal plant transfer function during the formation of the generalized plant and the controller. A block diagram of the generalized plant can be seen in Figure 21. As shown by Equations (4.9) and (4.10), the P matrix is portioned into four elements (P_{11}, P_{12}, P_{21}, and P_{22}). The column partitions correspond to exogenous inputs from the uncertainty matrix $\hat{\Delta}$, i.e. w (commands, disturbances, and noise), and the row partitions correspond to the exogenous outputs to the $\hat{\Delta}$ matrix, i.e. z (error signals to be minimized) [28]. This is to say that P_{11} has dimensions $a \times b$, where a and b are the number of inputs and outputs of $\hat{\Delta}$, respectively.

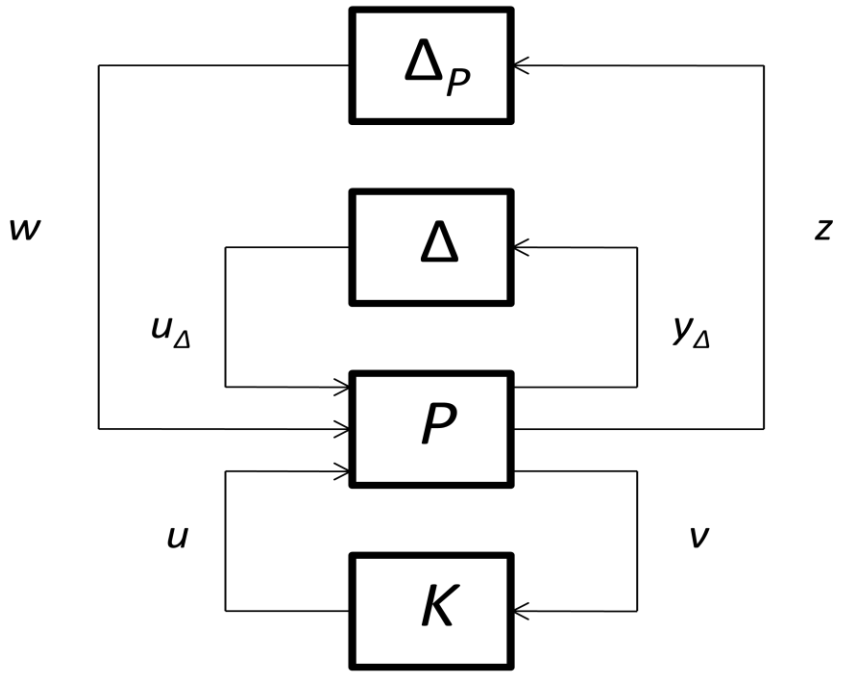

Figure 21. Block diagram of generalized plant

Using the generalized plant, a controller *K* was designed such that the H_∞ norm between the inputs and outputs of *N* are minimized to be less than one. It should be noted that the minimization is over the set of controllers that stabilize the control system. The Matlab® program *hinfsyn.m* is used produce a suitable H_∞ controller. The resulting controller transfer functions can be seen in Table 6.

Table 6. H_∞ Controller Transfer Functions

Uncertainty/Control	Controller Transfer Function
Multiplicative Velocity	$K_{hinf} = \frac{3.417e4s^4+1.316e6s^3+1.335e7s^2+6.11e7s+1.407e8}{s^5+2.437e4s^4+3.161e5s^3+1.61e6s^2+4.224e6s+7.411e5}$
Additive Velocity	$K_{hinf} = \frac{3774s^4+7.463e4s^3+5.912e5s^2+2.485e6s+4.9e6}{s^5+7306s^4+1.035e5s^3+5.646e5s^2+1.702e6s+3.015e5}$
Multiplicative Position	$K_{hinf} = \frac{3.443e4s^7+3.712e6s^6+6.987e7s^5+5.719e8s^4+2.235e9s^3+3.457e9s^2+1.703e5s+2.098}{s^8+3571s^7+4.771e5s^6+1.68e7s^5+1.373e8s^4+3.538e8s^3+6.194e7s^2+3060s+0.6768}$
Additive Position	$K_{hinf} = \frac{3.146e4s^4+8.802e5s^3+1.334e4s^2+109.1s+0.0005374}{s^5+4494s^4+4.585e5s^3+9.32e4s^2+1365s+10.8}$

The previously mentioned designed controllers for the velocity control objective resulted in extremely fast poles in the controller, K_{hinf}, for both multiplicative and additive cases, 3883Hz and 1160Hz, respectively. For this reason, model order reduction was performed. "The DC gain is the ratio of the output of the system to its input (presumed constant) after all transients have decayed" [29]. When removing a pole, it is desirable for the DC gain of the original transfer function to match that of the reduced transfer function. Upon doing so, the Bode plots should match well, except for at high

frequencies due to the removal of the pole. This is illustrated for the multiplicative and additive cases in Figure 23 and Figure 23, respectively. The resulting transfer functions are shown in Table 7.

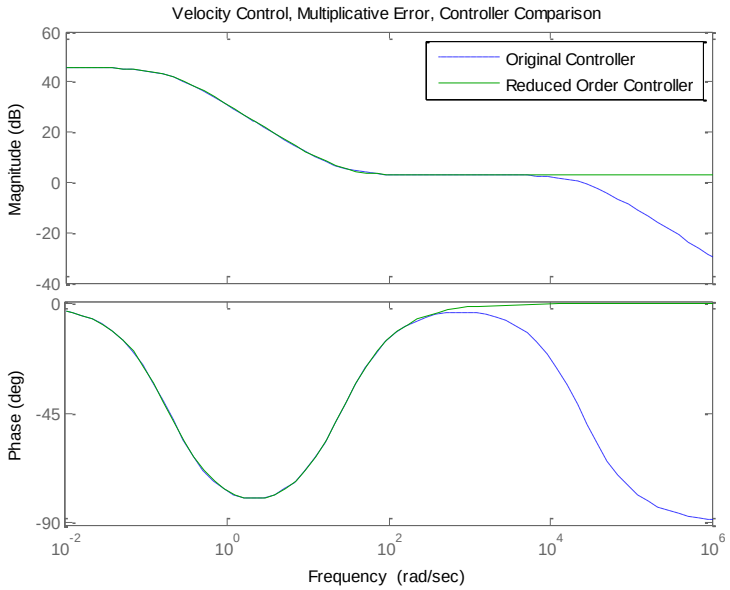

Figure 22. Bode comparison of multiplicative error controllers

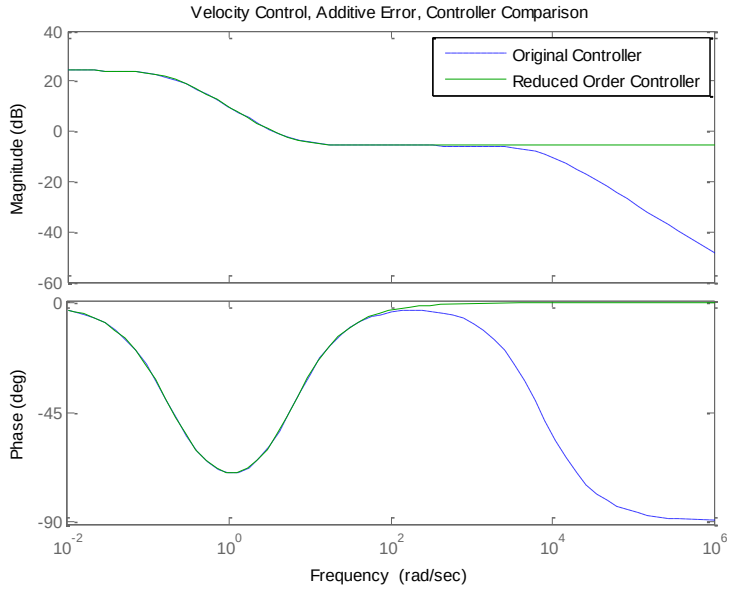

Figure 23. Bode comparison of additive error controllers

Table 7. Reduced Order Controller Transfer Functions

Uncertainty	Reduced Order Controller Transfer Functions
Multiplicative	$K_{hinf} = \frac{1.403s^4 + 54.05s^3 + 548.3s^2 + 2509s + 5779}{s^4 + 12.98s^3 + 66.09s^2 + 173.4s + 30.43}$
Additive	$K_{hinf} = \frac{0.5176s^4 + 10.23s^3 + 81.08s^2 + 340.8s + 672}{s^4 + 14.18s^3 + 77.4s^2 + 233.4s + 41.35}$

The structured $\hat{\Delta}$ matrix is considered when both uncertainty and performance are included in the controller design. The diagonal $\hat{\Delta}$ matrix is defined as

$$\hat{\Delta} = \begin{bmatrix} \Delta & 0 \\ 0 & \Delta_P \end{bmatrix} \tag{4.11}$$

where Δ is the model uncertainty and Δ_P is the performance uncertainty [28]. The Δ matrix has one input, y_Δ, and one output, u_Δ. The Δ_P matrix has two inputs, z_1 and z_2, and

one output, *w*. The controller has one input, *v*, and one output, *u*. With the generalized plant formed, the controller *K* can then be absorbed into the interconnection structure to obtain the system *N*, as shown in Figure 24. In other words, *N* is obtained by using *K* to close the lower feedback loop around *P*. The partitioned generalized plant and the controller are then transformed into the *N*-Δ configuration using the lower linear fractional transformation (LFT). From the LFT, *N* is defined by

$$N = P_{11} + P_{12}K(I - P_{22}K)^{-1}P_{21} \tag{4.12}$$

The *N* matrix is also portioned into four elements (N_{11}, N_{12}, N_{21}, and N_{22}). After *N* is computed and partitioned, standard robustness analysis is a simple task.

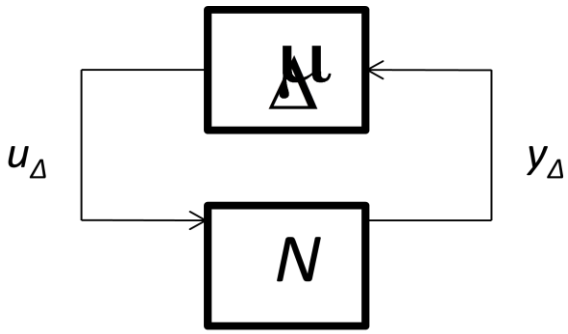

Figure 24. N- Δ Configuration

4.5 Defining Stability and Performance

Using the *N* and *P* matrixes, the conditions for stability and performance can be checked. To determine the stability and performance of the system an analysis must be performed. An analysis of nominal stability and performance determines the stability and performance of the nominal plant, respectively. A robust stability analysis determines whether the system remains stable for all plants in the uncertainty set, while a robust performance analysis determines how "large" the transfer function from exogenous input

w to outputs *z* may be for all plants in the uncertainty set [28]. In order to check for stability and performance, it is necessary to determine how they're defined.

- **Nominal Stability (NS):** Nominal stability implies that the system (i.e. nominal model) is stable without considering uncertainty [28]. In order to achieve this, *N* must be internally stable by only having poles in the left half plane (LHP).
- **Nominal Performance (NP):** In order for the system to achieve nominal performance, the nominal model must satisfy the performance specifications without model uncertainty [28]. The system must be nominally stable. The maximum singular value, $\bar{\sigma}$, of N_{22} or the structured singular values, μ, must be less than one, as shown by

$$NP \Leftrightarrow \bar{\sigma}(N_{22}) = \mu_{\Delta_P} < 1 \quad \forall \omega. \tag{4.13}$$

- **Robust Stability (RS):** Robust stability implies that the system is stable for all perturbed plants about the nominal model up to the worst-case model uncertainty [28]. The system must be nominally stable and the structured singular values of N_{11} must be less than one, as shown by

$$RS \Leftrightarrow \mu_{\Delta}(N_{11}) < 1 \quad \forall \omega. \tag{4.14}$$

- **Robust Performance (RP):** In order to achieve robust performance, the system must satisfy the performance specifications for all perturbed plants about the nominal model up to the worst-case model uncertainty [28]. The system must be nominally stable and the structured singular values of *N* must be less than one, as shown by

$$RP \Leftrightarrow \mu_{\hat{\Delta}}(N) < 1 \quad \forall \omega. \tag{4.15}$$

4.6 PID Control

A PID controller is also designed in order to compare to the H_∞ controller. The PID controller is expressed in the form

$$K_{PID} = K_P \left(1 + \frac{1}{K_I s} + K_D s \right), \tag{4.16}$$

where K_P, K_I, and K_D are the proportional, integral, and derivative controller gains, respectively. A PID controller is useful because it is capable of producing zero steady-state error while remaining stable, but can be difficult to tune due to the competing effects on the system response from adjusting the gains. The proportional gain is used to reduce rise time, the integral gain is used decrease steady-state error, and the derivative gain is used to reduce overshoot and settling time, but primarily to increase stability of the system. A balance must be met between each gain in order to achieve the desired performance requirements. The controller gains of K_P , K_I , and K_D that are found to provide the best performance can be seen in Table 8.

Table 8. PID Controller Gains

Motor Displacement	**Control Objective**	K_P	K_I	K_D
Fixed	Position	0.38	0.01	0.025
Fixed	Velocity	0.38	0.0001	0.025
Variable	Position	0.22	0.01	0.25
Variable	Velocity	0.38	0.0001	0.025

4.7 Conclusion

Throughout this chapter, the procedures for designing an H_∞ and a PID controller were outlined. The next step will be to run simulations that will test the controller's ability to resist external disturbances. The efficiency and performance of the robust controller will be compared to the PID controller. The results from the optimization method in the previous chapter, as well as the uncertainty analysis results, will also be presented in the next chapter. Finally, the variable displacement motor model will be compared to the fixed displacement motor model for a given work cycle to determine which system yields the greatest overall efficiency.

Chapter 5

RESULTS

5.1 Introduction

This chapter focuses on the H_∞ and a PID controller's ability to maximize efficiency and performance, while handling disturbances during a typical work cycle. These results are obtained through the use of simulations utilizing the Simulink® models presented in Chapter 2. The work cycle consists of having the excavator operate at low speeds when digging and dumping and high speeds when transferring the load or when the bucket is empty. A disturbance torque is added every time the excavator performs the operation of digging and transferring the load. The results of the optimization method described in Chapter 3 and the uncertainty analysis in Chapter 4 are also discussed.

5.2 Optimization Results

An optimization was performed in order to determine the best motor swash plate angle that resulted in the greatest overall efficiency. The results indicate that while it is not obvious, in some cases the system is more efficient when the motor is not at maximum displacement. This result typically occurred at low speeds and low torques, which can be seen in Figure 25. The only cases in which the greatest efficiency occurred at the maximum displacement for every load torque was for the 1:1 speed ratio. The change in oil temperatures also produced insignificant results. Any change in oil temperature from the original 60˚C produced a negligibly lower displacement that resulted in the same efficiency. The greatest difference in efficiency between the optimal and maximum motor displacement occurred during low loads and a speed ratio of 1:4 and

is shown in Figure 26. The 1:2 and 3:4 speed ratios produced a slight difference in efficiency between the optimal and maximum swash plate angle for low torques. An example of this is presented in Figure 27. Even though the difference in efficiency is small, it can still provide significant savings in energy over the lifetime of the pump. Finally, the 1:1 speed ratio produced the more obvious result of generating the greatest efficiency with the maximum swash plate angle, regardless of the output torque, and can be seen in Figure 28.

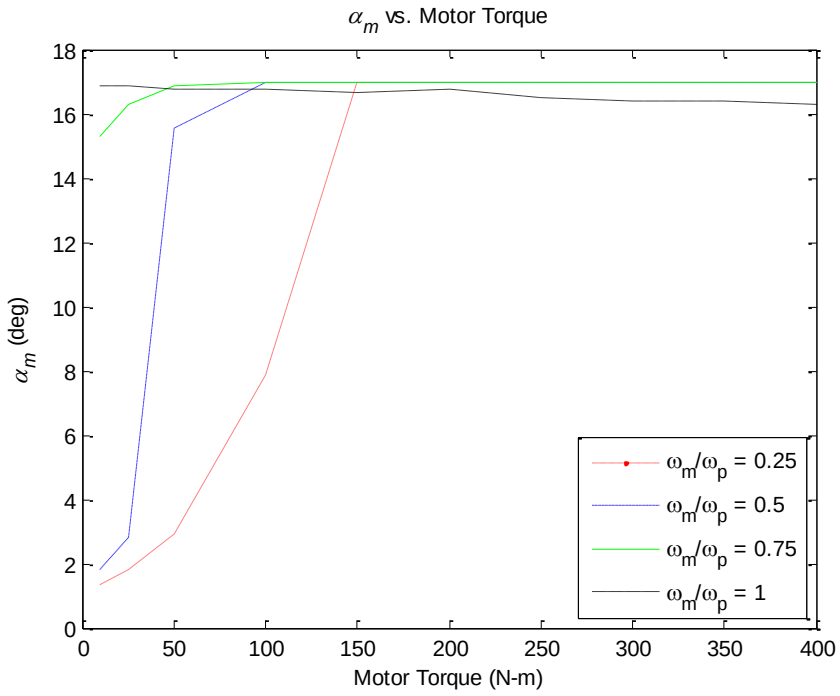

Figure 25. Optimal Motor Swash Plate Angles

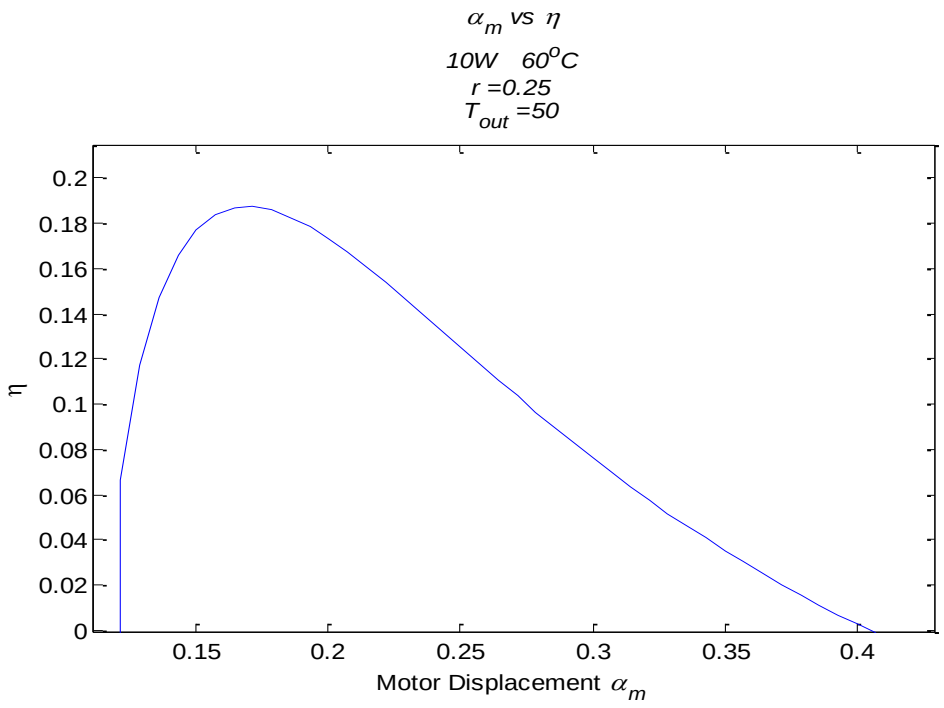

Figure 26. Optimal Motor Displacement - Low Speed, Low Load

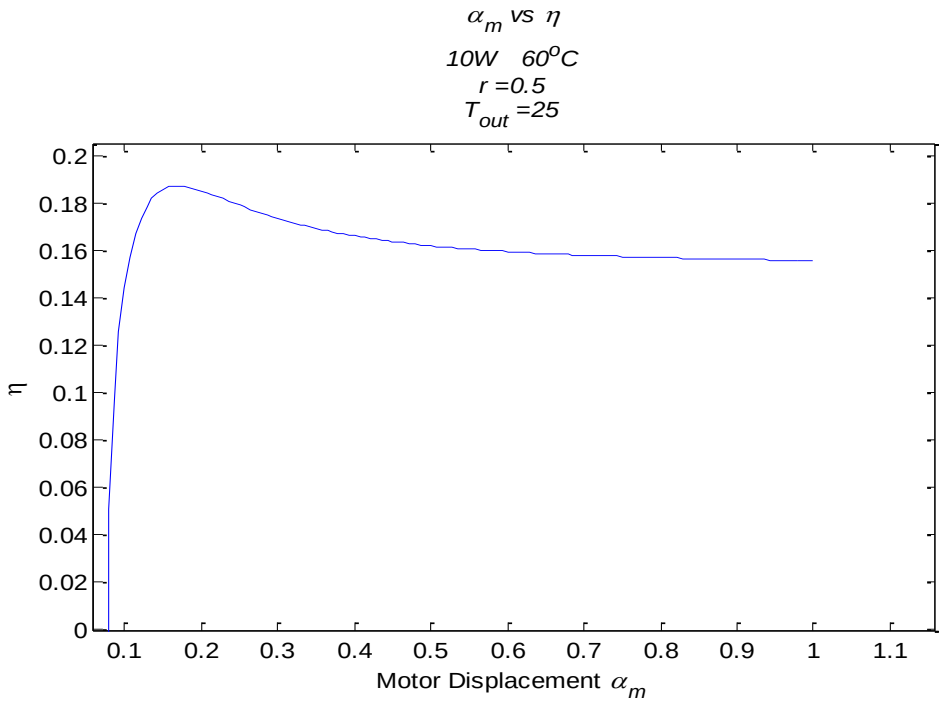

Figure 27. Optimal Motor Displacements - Medium Speed, Low Load

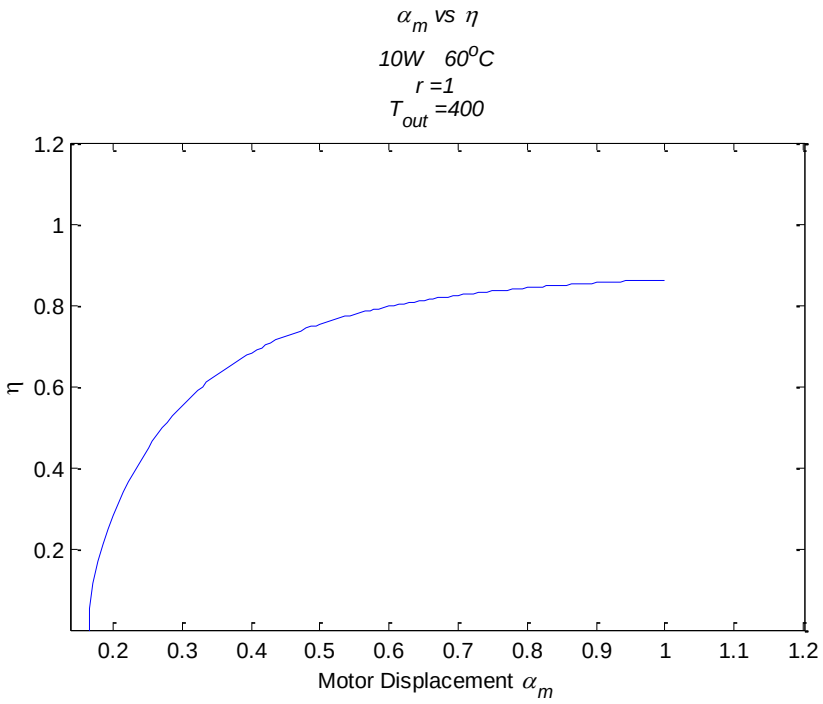

Figure 28. Optimal Motor Displacements - High Speed

5.3 Uncertainty Analysis Results

A robust controller is designed to maintain stability and performance under all expected operating conditions. The closed-loop control system must meet both a certain level of stability and performance. Nominal stability and performance correspond to the nominal plant, while robust stability and performance correspond to the perturbed plants. In order to meet nominal stability requirements, the closed loop system cannot have any right half plane poles. All poles were found to be in the left half plane, so all the systems were nominally stable. The structured singular value must be less than one, as shown in Equation (4.13), and the system must be nominally stable to achieve nominal performance. The structured singular values of N_{22} can be seen in Figure 29. The structured singular values are always less than one, so each system meets nominal

performance requirements. The inequality from Equation (4.14) must hold for all frequencies to achieve robust stability. The structured singular values of N_{11} can be seen in Figure 30. The structured singular values of N_{11} are below one for the entire frequency range, so each system is robustly stable. Finally, the structured singular values of N must be less than one to achieve robust performance, as seen in Equation (4.15). The structured singular values of N can be seen in Figure 31. The structured singular values of N are less than one, so each system meets robust performance requirements.

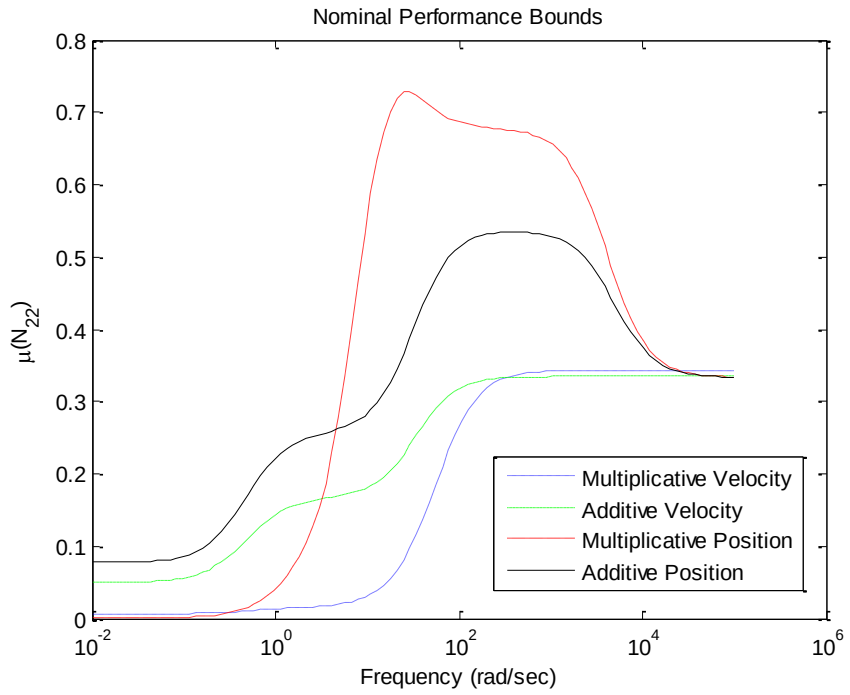

Figure 29. Nominal Performance Results

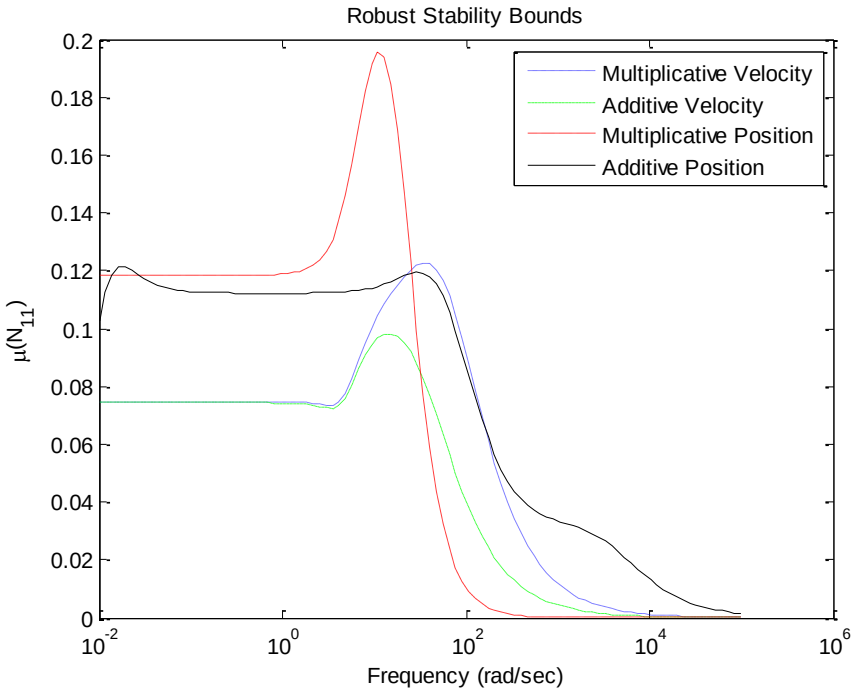

Figure 30. Robust Stability Results

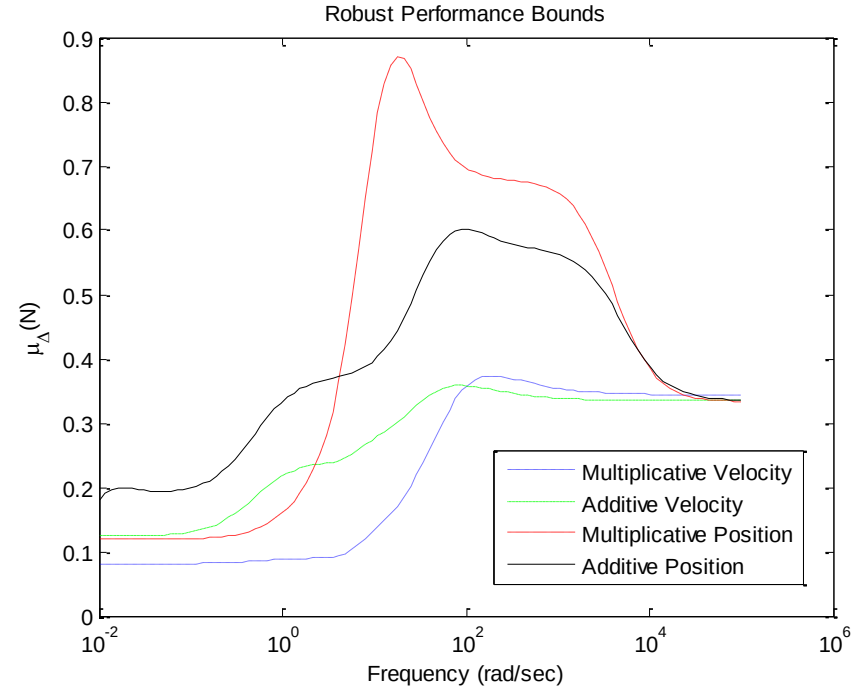

Figure 31. Robust Performance Results

5.4 Controller Comparison

PID and robust controllers were used to control the pump swash plate angle in order to achieve either the desired position or velocity. Both additive and multiplicative uncertainty cases were used in designing robust controllers. The robust controllers met the performance requirements for the position control objective, but both the additive and multiplicative robust controllers failed to reduce the steady state error. The robust controller used in the simulations was designed for only a partial range of varying parameters. Due to an extensive range of varying parameters, multiple robust controllers would need to be designed, as well as a way to smoothly switch control in order to generate a "bumpless" transfer and avoid undesirable transients. The control signals for each control system have saturation limits so that the swash plate does not go beyond its maximum and minimum range of motion. Going beyond the maximum range of motion would result in a physical inability of the swash plate, while allowing the control signal to go below the minimum range of motion would result in a reversal of fluid flow. The control signals of the robust controller and the PID controllers are shown in Figure 32 through Figure 35. The robust controller for the multiplicative uncertainty case produced undesirable results, as seen in Figure 35. Despite reducing the bandwidth frequency and performing model order reduction of the controller transfer function, the control system performed too fast and had a large overshoot. The robust controller for the additive uncertainty model and the PID controller for the fixed displacement position model had the least amount overshoot. All velocity controllers, with the exception of the additive robust controller and the PID position controllers, reach their saturation limits.

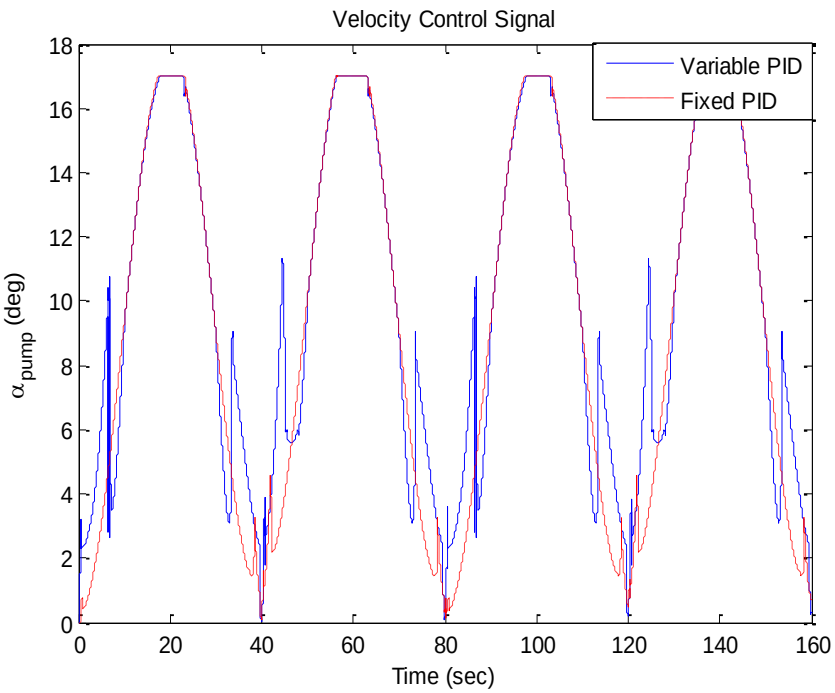

Figure 32. PID Control Signals - Velocity Control

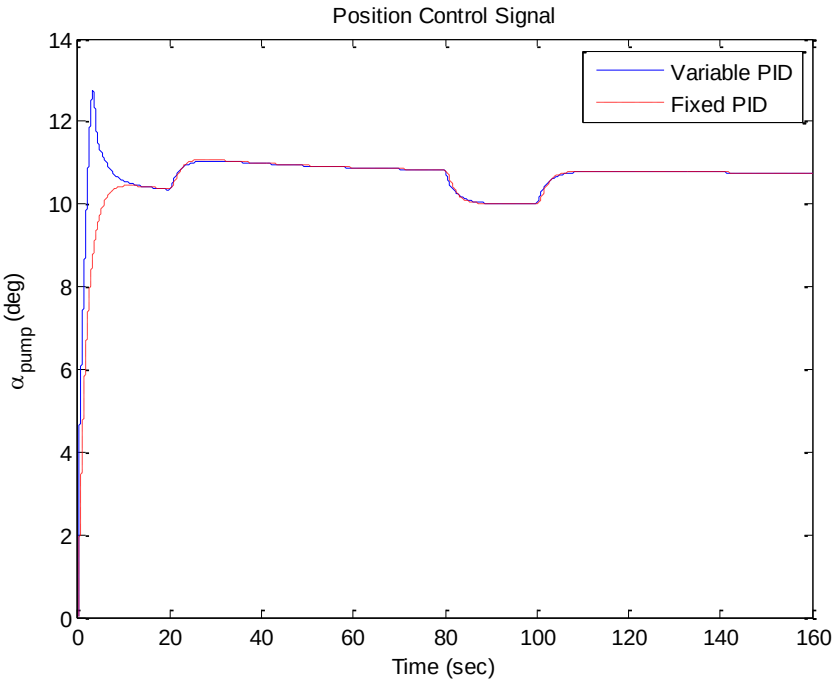

Figure 33. PID Control Signals - Position Control

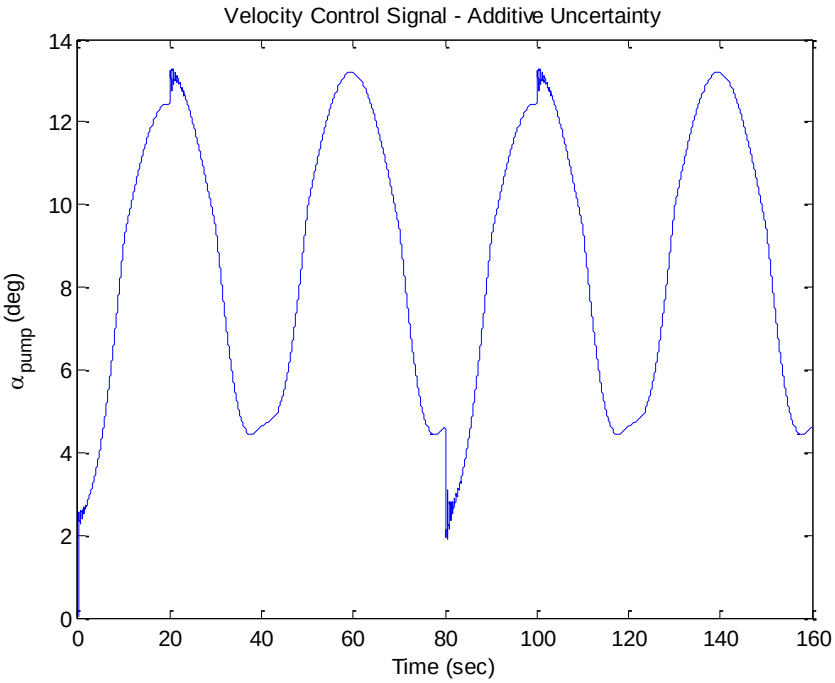

Figure 34. Robust Control Signal - Additive Error - Velocity Control

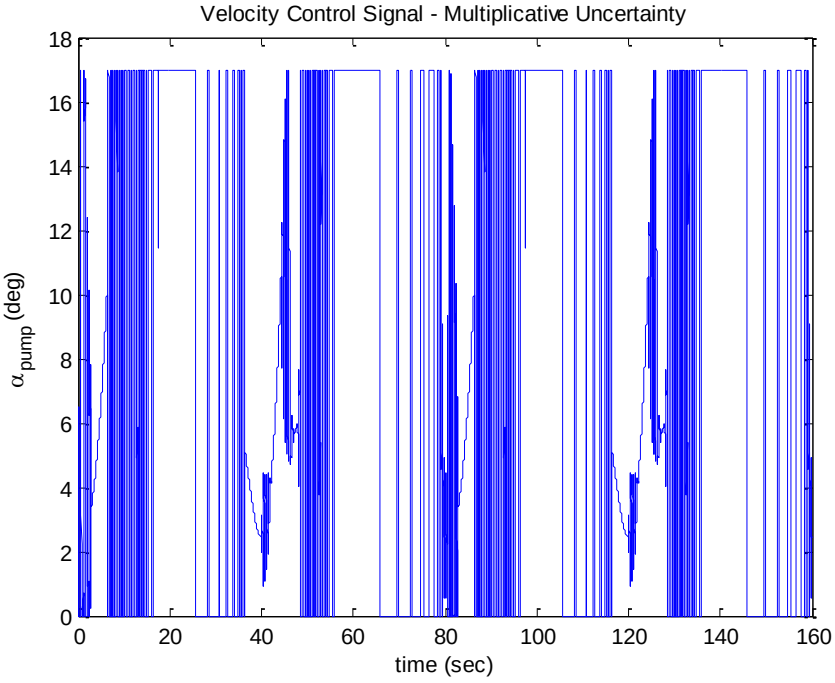

Figure 35. Robust Control Signal - Multiplicative Error - Velocity Control

5.5 Simulation Results

This section focuses on a scenario that tests the PID and H_∞ controller's ability to achieve either a desired position or velocity. The scenario will be simulated using a Simulink® model. With a focus on both efficiency and performance, these simulations demonstrate how well either position or velocity can be effectively maintained, as well as how efficient the variable displacement motor configuration is compared to the typical fixed displacement motor configuration. It should be noted that during the simulation development process, the Simulink® models were modified from their initial state. Due to a lack of back-pressure and a large inertia while operating under a small load torque, the motor failed to slow down to the desired velocity. In order to remedy this condition, the load torque was initiated twenty seconds sooner than shown in Figure 7. The initial motor displacement look-up table, Table 3, was also modified. In the instances that pressure became very large, the previously determined optimal motor displacement was not large enough to achieve the desired output torque. In order to counteract this situation, the motor swash plate angle was increased by approximately 6.5 degrees when the pressure reached 31.5 MPa and above for velocity control and approximately 3.4 degrees for position control. Lastly, in some cases, saturation of the pump swash plate caused the control signal to stop changing. The error signal continued to be applied to the integrator input, causing the integrator output of the PID controller to grow, or "wind up", until the sign of the error changed and the integration turned around. In order to combat this integrator windup, an anti-windup method was applied. The initial conditions for all simulations can be seen in Table 1. The simulation results of the

position control models will be presented first, followed by the results of the velocity control models.

Table 9. Simulation Initial Conditions

Parameter	Value
Pump Speed	2000 RPM
Motor Speed	0.01 RPM
Motor Position	0 rad
Pressure	10 MPa
Load Torque	25 N-m

The primary objective of the position control model is to accurately place the load at a specified location. This is typically done under slow moving conditions, therefore sacrificing speed for accuracy. As seen in Figure 36, both fixed and variable displacement motor models achieve the desired position in approximately 80 seconds. In approximately 3.5 seconds, the motor swash plate angle of the variable displacement motor model reaches its maximum limit of 17 degrees. This rapid acceleration to the saturation limit of the motor swash plate angle nullified any advantage of an adjustable swash plate. The fixed displacement motor model was also 2.43% more efficient than the variable displacement model, as seen in Figure 39. The cumulative efficiency, derived from Equations (2.1), (2.20), and (2.21), was determined by selecting the last data point from the efficiency results. These results confirm that for position control, the typical fixed displacement motor model is in fact more efficient.

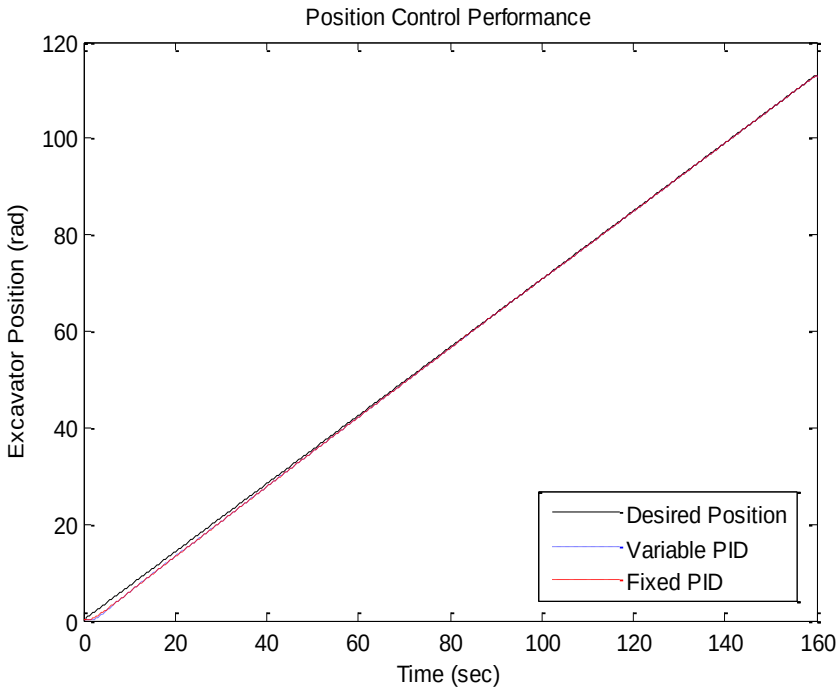

Figure 36. Position Control Performance Results

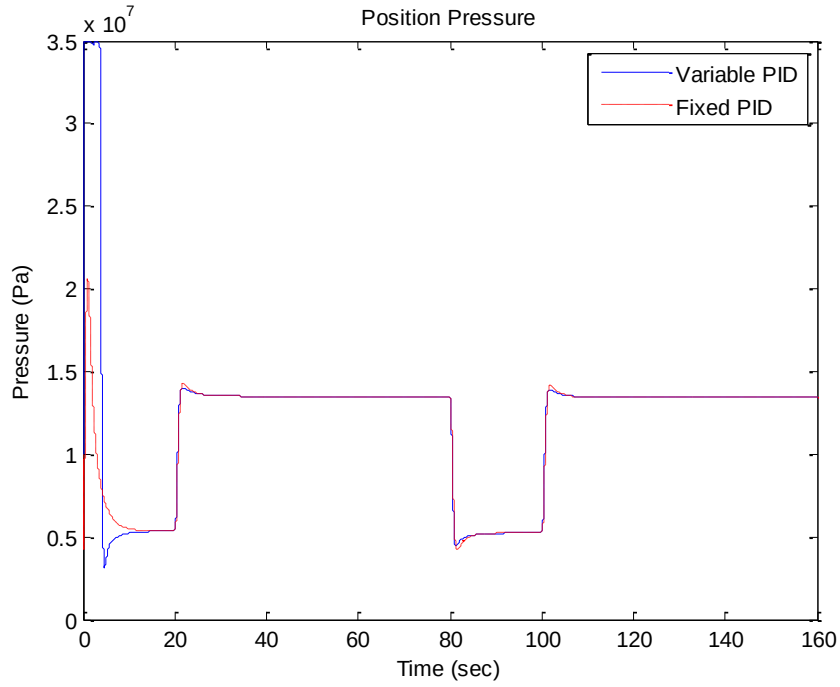

Figure 37. Position Control Pressure Results

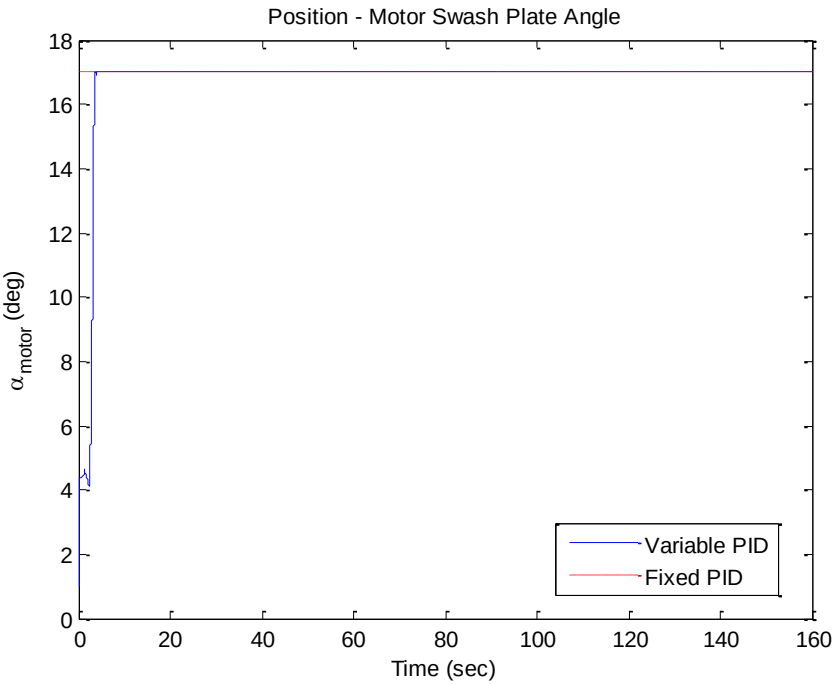

Figure 38. Position Control Motor Swash Plate Angle Results

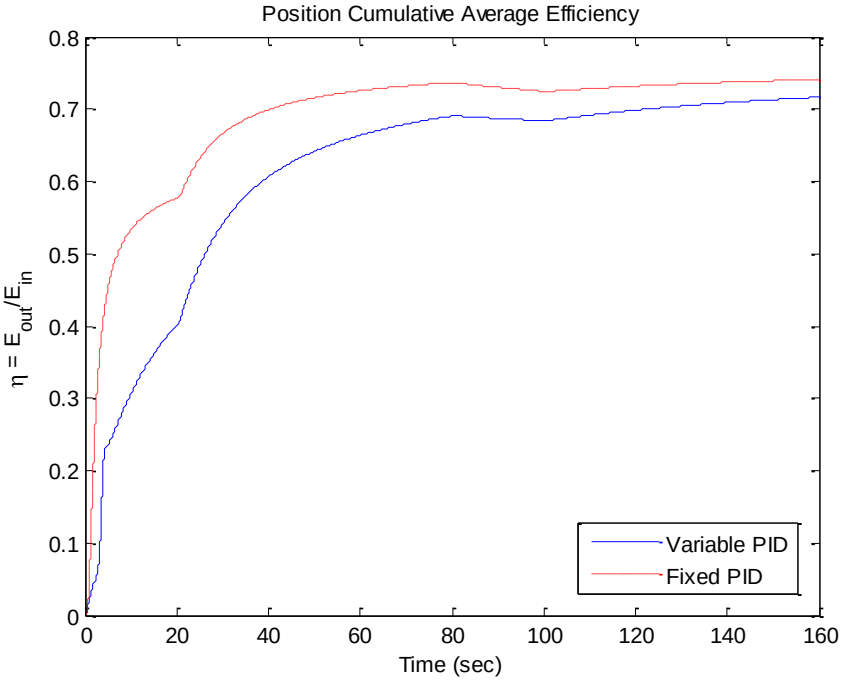

Figure 39. Position Control Efficiency Results

The primary objective of the velocity control model is to produce a specified output angular velocity for the load based on a desired angular velocity. As seen in Figure 40, both variable and fixed motor models fail to reach the upper limits of this desired velocity. Because of leakage, the system is not 100% efficient, and therefore struggles to reach the maximum desired velocity. Although it was unable to reach the desired velocity, the variable motor model exhibits slightly better performance than the fixed motor model. While the variable motor swash plate angle does reach its maximum limit, the majority of the work cycle is spent at a smaller angle. The variable displacement model was also 1.3% more efficient than the fixed displacement model, as shown by Figure 43. This difference in efficiency per work cycle, in terms of power and energy, can be seen in Table 10.

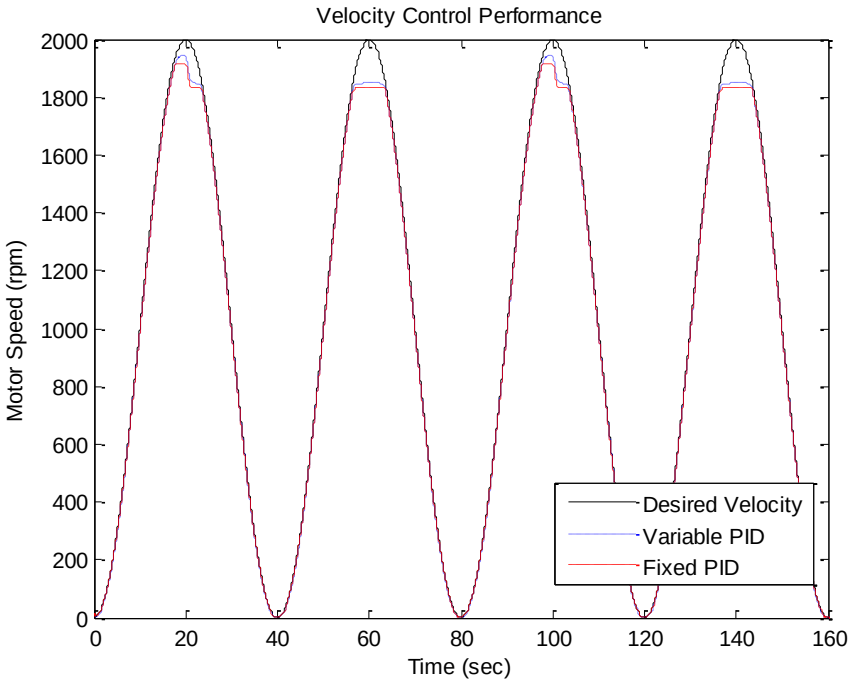

Figure 40. Velocity Control Performance Results

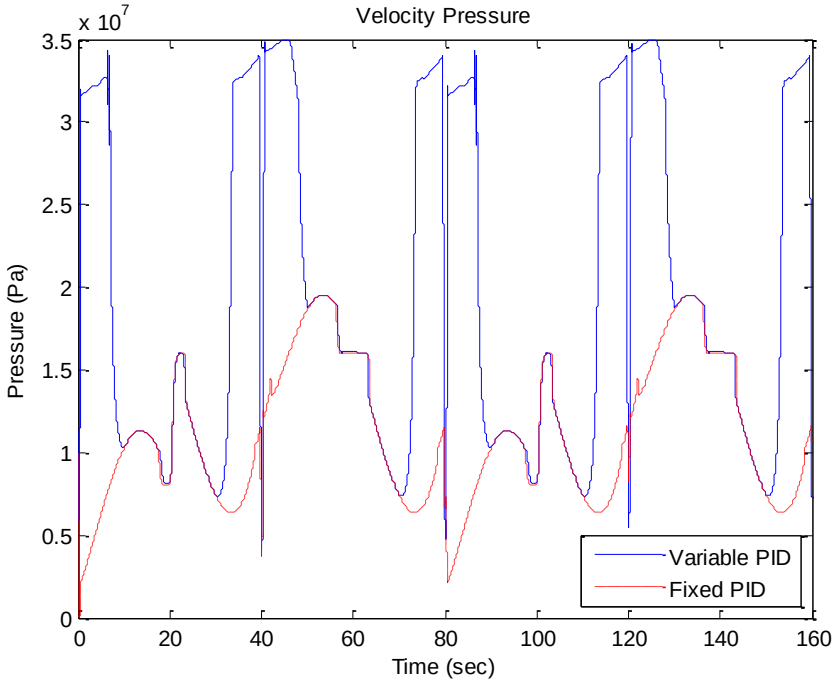

Figure 41. Velocity Control Pressure Results

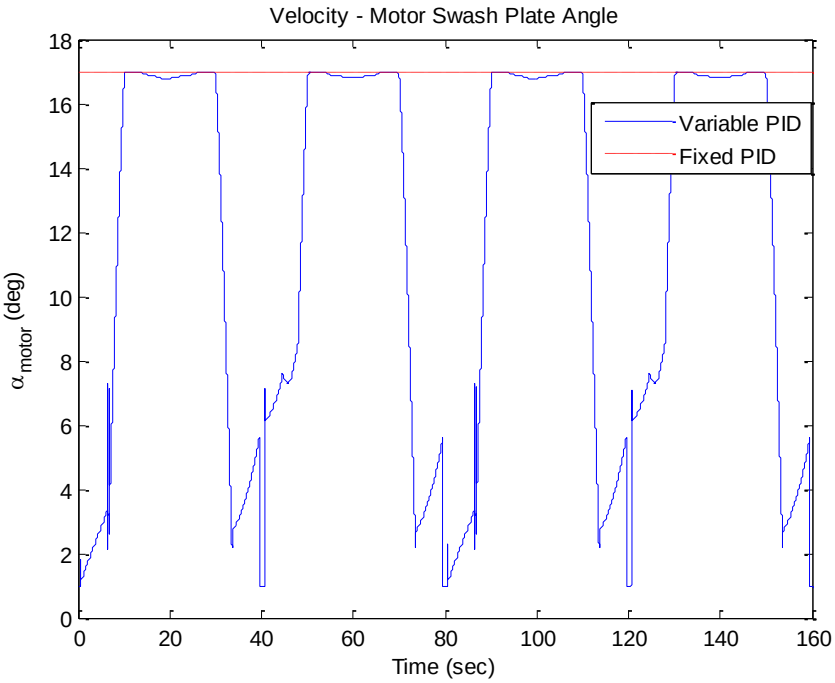

Figure 42. Velocity Control Motor Swash Plate Angle Results

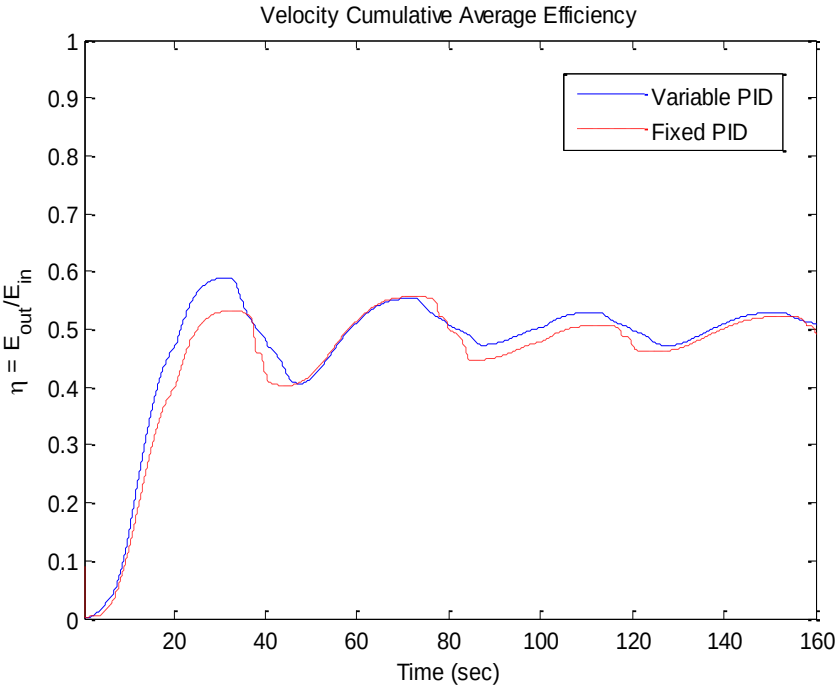

Figure 43. Velocity Control Efficiency Results

Table 10. Power and Energy Differences

Parameter	Value
Difference in Energy Input to System	360600 J
Difference in Energy Output by System	71200 J
Difference in Power Input to System	3.02 HP
Difference in Power Output by System	0.6 HP

Lastly, a robust controller was designed to control the velocity of the variable displacement motor. This controller was designed for a smaller range of operating conditions, specifically 600 to 1400 RPM. As stated previously, multiple controllers would be required to maintain performance for the full range of operating conditions. For the given set of operating conditions, a simulation using the previously designed PID controller was compared to the robustly controlled model. The robustly controlled model exhibited slightly better performance than the PID controlled model. As demonstrated in Figure 44, the actual velocity is nearly identical to the desired velocity. Much like the PID controlled variable displacement motor model, the motor swash plate angle of the robustly controlled model reached its maximum limit, but is at a lower angle for approximately half the work cycle. The robustly controlled variable displacement motor model was also 0.32% more efficient than the PID controlled model, as displayed in Figure 47. All efficiency results can be seen in Table 11.

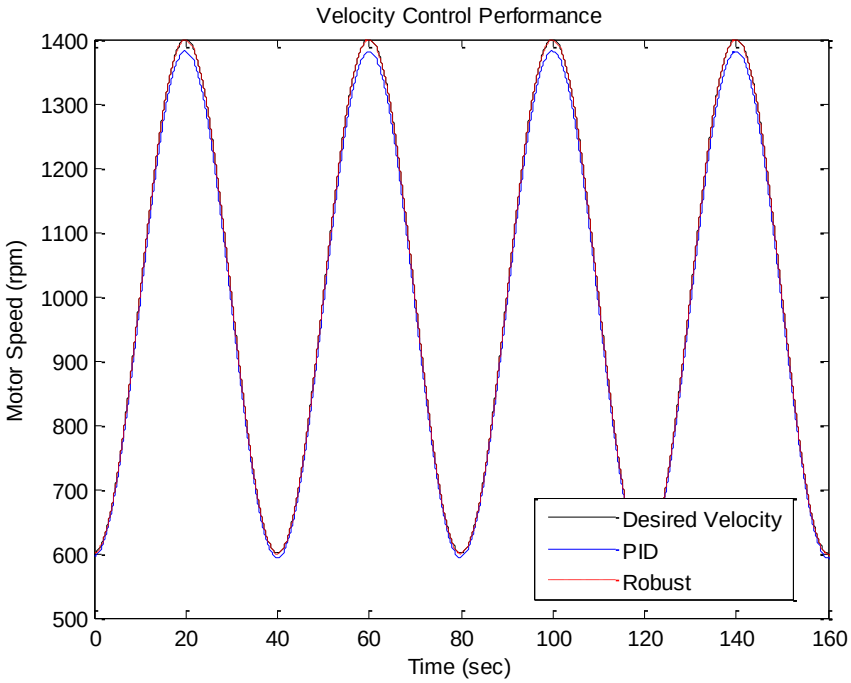

Figure 44. Velocity Control Performance Results - PID vs Robust

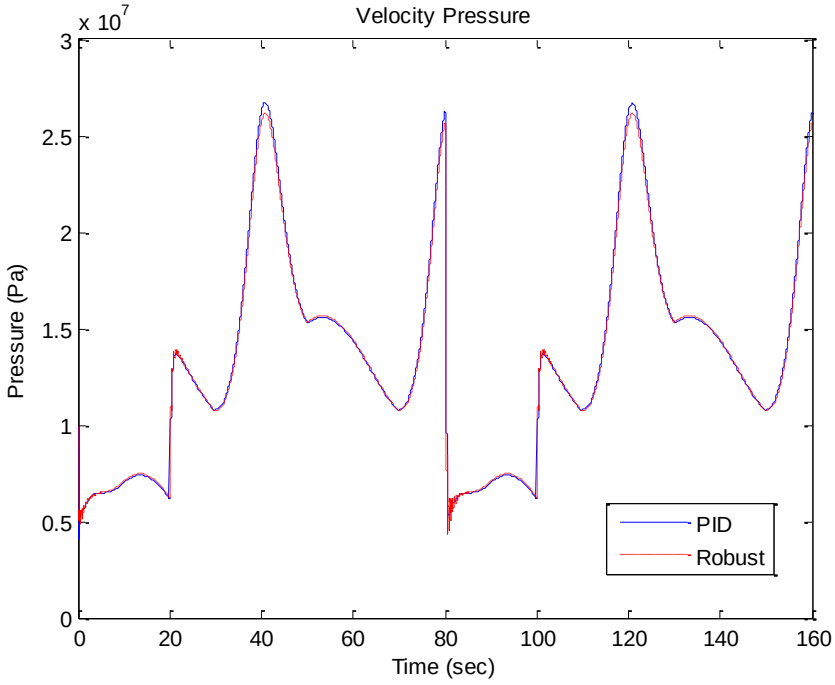

Figure 45. Velocity Control Pressure Results - PID vs Robust

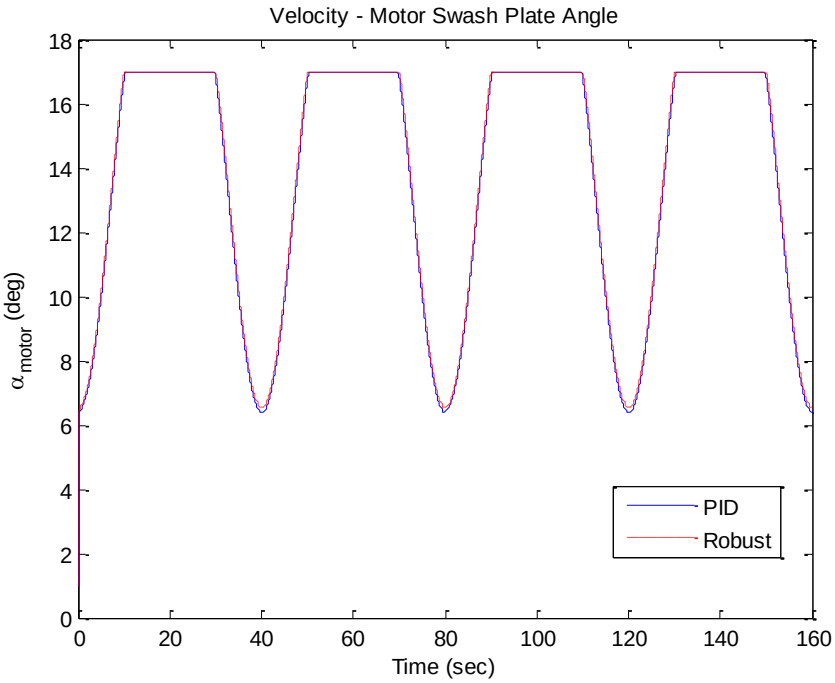

Figure 46. Velocity Control Motor Swash Plate Angle Results - PID vs Robust

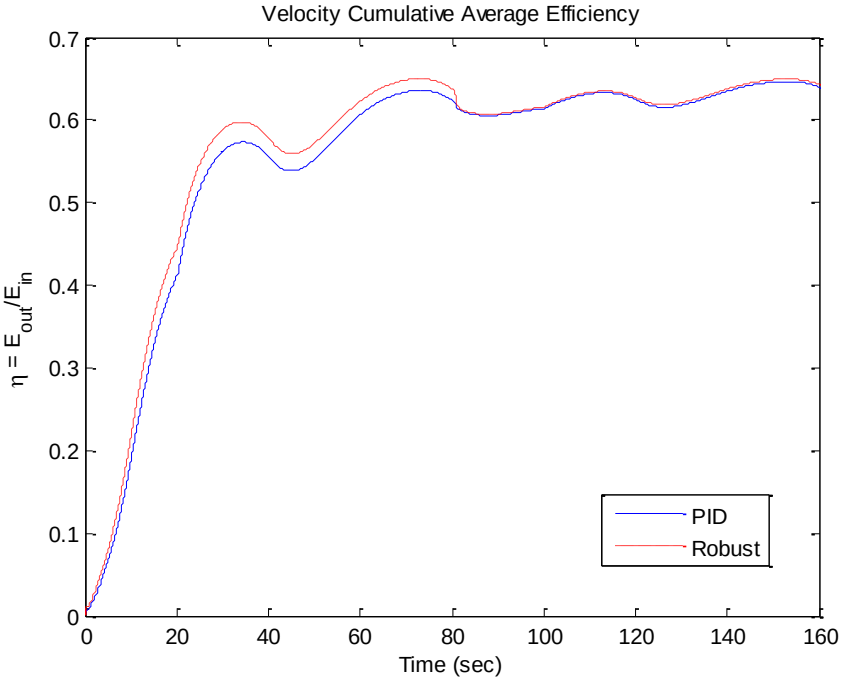

Figure 47. Velocity Control Efficiency Results - PID vs Robust

Table 11. Efficiency Results

Control Objective	Motor Type	Cumulative Efficiency
Position – PID	Fixed	74.08%
Position – PID	Variable	71.65%
Velocity – PID	Fixed	49.53%
Velocity – PID	Variable	50.83%
Velocity – Robust	Variable	64.38%
Velocity – PID (Robust Comparison)	Variable	64.06%

5.6 Conclusion

Throughout this chapter, the results of the motor swash plate optimization, uncertainty analysis, and the H_∞ and a PID controller's ability to maximize efficiency and performance, while handling disturbances during a typical work cycle, were presented. It has been shown that a variable displacement motor can, in fact, provide a greater efficiency than a fixed displacement motor. It has also been shown that a variable displacement motor can generate a greater efficiency than a fixed displacement motor for the typical work cycle of an excavator. A more extensive explanation of the results of this work will be discussed in the next chapter.

Chapter 6

CONCLUSION

6.1 Discussion

The purpose of this research has been to focus on increasing the performance and efficiency of a hydrostatic transmission utilizing a closed loop system and a variable displacement motor. Typically, most machines use open loop control to achieve a desired performance requirement. The equipment operator ultimately has control of the machinery, leaving the actual performance to a combination of his speed and accuracy. Because there is no electronic feedback signal to reduce the error, an open loop control system lacks the ability to affect the performance of the system in the way that a closed loop control system could. For a typical hydrostatic transmission, a fixed displacement motor is used in combination with a variable displacement pump. The maximum swash plate angle of the motor is set to produce the largest amount of torque required, thus making the system most efficient when operating under this condition. While the system may be most efficient when outputting the peak amount of torque, it is very inefficient when a small amount of torque is required. This occurs when the excavator bucket is empty, which accounts for half of the work cycle. These problems have made it advantageous to investigate the use of a closed loop system and a variable displacement motor that would not only be better suited to increasing performance, but also better efficiency.

Before a simulation of the typical work cycle for a Caterpillar 320D excavator utilizing a variable displacement motor could be performed, it was necessary to establish

an analytical model of a hydrostatic transmission. Next, it was essential to determine the most advantageous motor swash plate angle that would maximize efficiency for a given output torque. While maintaining a constant pump speed, an optimization was performed to determine the best motor swash plate angle that resulted in the greatest efficiency. This optimization showed that in some explicit cases, specifically low speed and low torque, the system could produce a greater efficiency with a less than maximum swash plate angle.

Next, a model was developed that would fully describe the typical work cycle of a excavator employing a hydrostatic transmission with both a variable displacement pump and motor. This model consists of a work cycle that would include a disturbance torque when transferring a bucket that was either empty or full of material debris. The model also includes an accurate model of a hydrostatic transmission's pump, motor, and connecting hoses, and an efficiency model that would determine the cumulative average efficiency of the hydraulic system.

Both and PID and robust control schemes were developed for the excavator, and both controller designs were able to provide suitable performance, while simultaneously creating stability, good damping, and a quick response. Extensive adjustments, along with numerous attempts, were utilized in order to determine PID gains, as well as bandwidth frequency, low frequency error, high frequency error, performance weights, and controller effort weights for a suitable H_∞ controller.

Numerical simulations were performed to demonstrate the performance and efficiency. The performance of two control objectives, position control and velocity control, were tested. Both additive and multiplicative error models were used in the

development of robust controllers. While both types met robust stability and robust performance requirements for both control objectives, only the additive error model for the velocity control objective produced desirable results.

For position control, both fixed and variable displacement motor models produced the highest cumulative average efficiency. These high efficiencies are most likely due to the slow speed at which the motor rotated, a common characteristic of position control, and the fact that low operating speeds produced greater efficiencies for the motor swash plate optimization. While the most favorable motor swash plate angles were applied, a slight increase in swash plate angle was supplemented when the pressure reached 31.5 MPa. The need for a supplemental swash plate angle is likely due to the limit number of data points used in the optimization. The position controls models did not exhibit the fastest response; however, they did provide the best performance upon acquiring the desired objective over the course of the entire operating range.

For velocity control, the fixed and variable displacement motor models were compared, as well as the PID controlled model and the robustly controlled model. Similar to the position control models, the motor swash plate angle was increased when the pressure reached 31.5 MPa. The robustly controlled model was conducted over a smaller range of operating conditions. The robust model performed better than the comparable PID controlled model and was slightly more efficient. With the addition of multiple robust controllers and a "bumpless" transition between them, the robustly controlled model has the potential to perform the best and obtain the greatest efficiency for the entire range of operating conditions.

Lastly, for velocity control, the fixed displacement motor model was compared to the variable displacement motor model. The variable model performed slightly better than the fixed model. Although each model performs well, neither could reach the upper desired speed limit, most likely because the pump reaches the maximum flow limit and each controller reaches its saturation limit. When the system saturates, the effectiveness (i.e. the performance) of the control system is diminished. The variable displacement model is also more efficient than the fixed displacement model. When the savings in energy are extrapolated over the lifetime of the pump, a significant amount of energy is accumulated. The 1.3% increase in hydraulic efficiency also expands to an even greater amount of energy savings for the entire system when the internal combustion engine driving the pump is taken into account. The increase in efficiency of the variable displacement motor has the potential to offset its additional cost. It should also be noted that while the velocity control does not exhibit as great of efficiency as position control, the two cannot easily be compared due to the fact that the position control model operated at a much lower speed, and in general, very different operating conditions.

A typical hydrostatic transmission combines a variable displacement pump and a fixed displacement motor. With the method discussed in this paper, a variable displacement motor replaces the fixed displacement motor and a smaller swash plate angle is utilized to achieve a greater hydraulic efficiency. While this method is not a common means of operation, this research has determined that even though it is not obvious, a hydraulic system can be more efficient when the motor is not at maximum displacement through the use of a variable displacement motor.

6.2 Future Work

The analysis of the system can be investigated further by varying the pump speed, allowing reversible flow, creating more robust controllers and a "bumpless" transition between them, but most importantly an experiment replicating the previously described numerical model. Allowing the pump speed to vary could result in more cases or higher efficiencies with a less than maximum motor swash plate angle. Permitting the pump and motor swash plates to move down to -17 degrees would allow the system to be reversible. Reversible flow would enable the excavator to move back and forth by quarter turns instead of rotating a full 360 degrees as depicted in this work. Reversible flow would also allow the development of backpressure, therefore enabling the excavator to slow more effectively. This reversal of fluid flow could not only improve performance, but efficiency as well. The robust controller displayed potential for the best performance and the greatest efficiency. The development of more robust controllers to accommodate the entire operating range and a "bumpless" transition between them could result in both a better performance and a greater efficiency than the PID controlled model. Finally, an experiment replicating the previously described numerical model could be conducted. An experiment would be much more involved than the numerical model outlined in this thesis, but would show more accurate efficiency and performance results.

BIBLIOGRAPHY

[1] *Hydraulics: The Fundamentals of Service and Theory of Operation for Hydraulic Systems in Off-Road Vehicles, Trucks, and Buses.* Moline, IL: John Deere Publishing, 2006.

[2] N. D. Manring, *Hydraulic Control Systems*. Hoboken, NJ: John Wiley & Sons, Inc., 2005.

[3] J. Watton, *Fundamentals of Fluid Power Control*. New York: Cambridge University Press, 2009.

[4] R. P. Lambeck, *Hydraulic Pumps and Motors: Selection and Application for Power Control Systems*. New York: Marcel Dekker, Inc., 1983.

[5] A. Akers, *et al.*, *Hydraulic Power System Analysis*. Boca Raton, FL: Taylor & Francis Group, 2006.

[6] H. L. Stewart, *Hydraulics for Off-the-Road Equipment*, Second ed. Boston, MA: G.K. Hall & Co., 1985.

[7] W. E. Wilson, *Positive Displacement Pumps and Fluid Motors*. New York: Pitman Publishing Corporation, 1950.

[8] W. M. J. Schlosser, "Mathematical Model for Displacement Pumps and Motors " *Hydraulic Power Transmission*, pp. April, 252-257 and 269, and May, 324-328, 1961.

[9] W. M. J. Schlosser, "The Overall Efficiency of Positive Displacement Pumps," *Fluid Power Symposium*, pp. 34-48, 1968.

[10] X. Shi and N. D. Manring, "A Torque Efficiency Model for an Axial-Piston, Swash-Plate Type, Hydrostatic Pump," *Bath Workshop on Power Transmission and Motion Control*, pp. 3-20, 2001.

[11] J. Thoma, "Mathematical Models and Effective Performance of Hydrostatic Machines and Transmissions," *Hydraulic Pneumatic Power*, pp. 642-651, 1969.

[12] H. E. Merritt, *Hydraulic Control Systems*. New York: John Wiley & Sons, Inc., 1967.

[13] J. Thoma, *Hydrostatic Power Transmission*. Surrey, England: Trade and Technical Press, 1964.

[14] G. a. A. Zeiger, "Torque on the Swashplate of an Axial Piston Pump," *ASME Journal of Dynamic Systems, Measurement, and Control*, vol. 107, pp. 220-226, 1985.

[15] G. a. A. Zeiger, "Dynamic Analysis of an Axial Piston Pump Swashplate Control," *Journal Proceedings of the Institution of Mechanical Engineers*, vol. 200, pp. 49-58, 1986.

[16] N. D. Manring and R. E. Johnson, "Modeling A Variable Displacement Pump," in *ASME Fluids Engineering Division Summer Meeting*, Lake Tahoe, Nevada, 1994, pp. 1-10.

[17] *Hydraulics and Pneumatics: Hydrostatic Transmissions*. Available: http://www.hydraulicspneumatics.com/200/TechZone/HydraulicPumpsM/Article/True/6450/TechZone-HydraulicPumpsM

[18] N. D. Manring and G. R. Luecke, "Modeling and Designing a Hydrostatic Transmission With a Fixed-Displacement Motor," *Journal of Dynamic Systems, Measurement, and Control*, vol. 120, pp. 45-49, 1998.
[19] J. T. Peterson, *et al.*, "Directional Control of a Dual-Path Hydrostatic Transmission for a Track-Type Vehicle," *Proceedings of the ASME Fluid Power Systems and Technology Division*, vol. 11, pp. 147-156, 2004.
[20] T. H. Ho and K. K. Ahn, "Modeling and Simulation of Hydrostatic Transmission System With Energy Regeneration Using Hydraulic Accumulator," *Journal of Mechanical Science and Technology*, 2010.
[21] S. Hui, *et al.*, "Factors Influencing the System Efficiency of Hydostatic Transmission Hybrid Vehicles," *IEEE Vehicle Power and Propulsion Conference*, 2008.
[22] J. Van de Ven, *et al.*, "Development of a Hydro-Mechanical Hydraulic Hybrid Drive Train with Independent Wheel Torque Control for an Urban Passenger Vehicle," presented at the International Exposition for Power Transmission, 2008.
[23] *Vickers Industrial Hydraulics Manual*, Third ed. Rochester Hills, MI: Vickers, Incorporated, 1993.
[24] (12/22/10). *Kurt Hydraulics: High Pressure Hydraulic Lines*. Available: http://www.kurthydraulics.com/products.php?10=&11=&12=830&13=1247&15=1734&16=1964&17=2001&18=2003&category=156
[25] "Caterpillar 320D Hydraulic Excavator," ed: Caterpillar, 2007.
[26] N. D. Manring, "Analysis, Design, and Control of Axial Piston Swash-Plate Type Hydrostatic Machines," unpublished|, 1998.
[27] K. Ogata, *System Dynamics*, Fourth ed. Upper Saddle River: Pearson Prentice Hall, 2004.
[28] S. a. P. Skogestad, I., *Multivariable Feedback Control: Analysis and Design*, Second ed.: John Wiley and Sons, Ltd, 2005.
[29] G. F. Franklin, *et al.*, *Feedback Control of Dynamic Systems*, Fifth ed. Upper Saddle River: Pearson Prentice Hall, 2006.

APPENDIX

Parameters	Value
Pump Speed	1800 RPM
Speed Reduction Ratio	166:1
Max Flow Rate	280 LPM
Leakage	10%
Viscosity	0.15 Pa-s
Excavator Mass	50,000 kg
Secant Bulk Modulus of Mineral Oil	1560 MPa
Slope of Increase of Mineral Oil	5.6
Elastic Modulus of Flexible Hose	5900 MPa
Poisson's Ratio of Flexible Hose	0.47
Hose O.D.	0.0498 m
Hose I.D.	0.0318 m
Hose length	2.7432 m
Max Pressure	35 MPa
Viscous Drag Coefficient	1.2266E-16 N-m-s
Moment of Inertia	7.2579 kg-m^2
Excavator Boom Length	4 m
Excavator Swing Speed	11.5 RPM
Excavator Swing Torque	61.8 kN-m
Pump – Cl	4.1990E-9

Pump – Ct	1.6867E-6
Pump – Cs	9.5492E-4
Pump – Cc	2.2229E5
Pump – Ch	22.4496
Motor – Cl	4.4645E-9
Motor – Ct	-4.2887E-6
Motor – Cs	0.2400
Motor – Cc	1.5341E6
Motor - Ch	-1.0899E3